THE UNIVERSITY of EDINBURGH

# Edinburgh Research Explorer

# A process-based model for ammonia emission from urine patches, GAG (Generation of Ammonia from Grazing): description, validation and sensitivity analysis

OPEN ACCESS

# A process-based model for ammonia emission from urine patches, GAG (Generation of Ammonia from Grazing): description and sensitivity analysis

Andrea Móring[1,2,3], Massimo Vieno[2], Ruth M. Doherty[1], Johannes Laubach[4], Arezoo Taghizadeh-Toosi[5], and Mark A. Sutton[2]

[1]School of GeoSciences, University of Edinburgh, Crew Building, Alexander Crum Brown Road, Edinburgh, EH9 3FF, UK
[2]NERC, Centre for Ecology & Hydrology, Edinburgh, Bush Estate, Midlothian, Penicuik, EH26 0QB, UK
[3]Hungarian Meteorological Service, Kitaibel P. u. 1, 1024 Budapest, Hungary
[4]Landcare Research, P.O. Box 69040, Lincoln 7640, New Zealand
[5]Department of Agroecology, Aarhus University, Blichers Allé 20, 8830 Tjele, Denmark

*Correspondence to:* Andrea Móring (a.moring@sms.ed.ac.uk)

**Abstract.** In this paper a new process-based, weather-driven model for ammonia (NH$_3$) emission from a urine patch has been developed and its sensitivity to various factors assessed. The GAG model (Generation of Ammonia from Grazing) is capable of simulating the TAN (total ammoniacal nitrogen) and the water content of the soil under a urine patch and also soil pH dynamics. The model tests suggest that ammonia volatilization from a urine patch can be affected by the possible restart of urea hydrolysis after a rain event as well as CO$_2$ emission from the soil. The vital role of temperature in NH$_3$ exchange is supported by our model results; however, the GAG model provides only a modest overall temperature dependence in total NH$_3$ emission compared with the literature. This, according to our findings, can be explained by the higher sensitivity to temperature close to urine application than in the later stages and may depend on interactions with other nitrogen cycling processes. In addition, we found that wind speed and relative humidity are also significant influencing factors. Considering that all the input parameters can be obtained for larger scales, GAG is potentially suitable for field and regional scale application, serving as a tool for further investigation of the effects of climate change on ammonia emissions and deposition.

## 1 Introduction

The consequences of strong emission of reactive nitrogen compounds (N$_r$), dominated by the emission of ammonia (NH$_3$), are widely discussed: threatening air, water and soil quality, it endangers also ecosystems as well as human health in many ways (Sutton et al., 2011; Galloway et al., 2008; Fowler et al., 2013). Globally 70 % of NH$_3$ released to atmosphere originates from agricultural sources, such as livestock housing, manure management, and fertilizer spreading on fields (EDGAR, 2011). According to the latest available report of the UK government agency DEFRA (Department for Environment, Food and Rural Affairs), in the UK grazing accounts for ca. 11 % of the total NH$_3$ emission (Misselbrook et al., 2012). Although this proportion in the total national emission is rather small, since two thirds of the grasslands are estimated to be grazed (Hellsten et al., 2008), NH$_3$ emission from grazing affects a significant percentage of the country.

As demonstrated by both laboratory and field experiments (Farquhar et al., 1980; Sutton et al., 1995), ammonia exchange between atmosphere and surface is a bidirectional process and dependent largely on meteorological factors, especially temperature. The direction of the net NH$_3$ exchange at any time depends on the relative magnitude of the ambient air concentration of NH$_3$ high above the surface and the concentration of NH$_3$ right above the surface (referred to as the "compensation point"). If the air concentration is the larger

of the two, deposition occurs; whilst in the opposite case, emission takes place.

During grazing, the dominant $NH_3$ source is urine, rather than dung (Petersen et al., 1998; Laubach et al., 2013). In a urine patch ammonium ($NH_4^+$) is produced by urea hydrolysis. Because of the equilibrium between $NH_4^+$ and $NH_3$, increasing $NH_4^+$ concentration results in an $NH_3$ compensation point that is usually higher than the ambient air concentration above the urine patch. This generally leads to $NH_3$ emission from a urine patch. According to the literature (e.g. Sherlock and Goh, 1985; Laubach et al., 2012 and the references therein) the period with significant $NH_3$ emission lasts about 4–8 days after urine deposition.

The state-of-the-art $NH_3$ exchange models for vegetated surfaces (e.g. Burkhardt et al., 2009; Flechard et al., 2013), called canopy compensation point models, use the analogy of electrical circuits. In these, electrical current and potential difference represent $NH_3$ fluxes and the difference between the $NH_3$ concentrations at the different levels of the canopy, respectively. The model resistances capture the influence of meteorological factors and the canopy on $NH_3$ transfer. The first "canopy compensation point" model (Sutton et al., 1995) took into account the net $NH_3$ exchange with vegetation (a single-layer model), considering exchange with stomata and leaf surfaces. Later the canopy compensation point approach was developed by including $NH_3$ exchange also with soil surface (a two-layer model by Nemitz et al., 2001) and different parts of the plant, such as siliques and foliage (a three-layer model by Nemitz et al., 2000).

An example for estimating emissions from an excretal source that applies a simple compensation point model is the GUANO model (Riddick, 2012; Sutton et al., 2013), which simulates the processes leading to $NH_3$ emission from seabird excreta. In this model the compensation point is calculated based on Henry's law (for partitioning of $NH_3$) and the dissociation of $NH_4^+$ over a hypothetical surface covered by guano. In calculating the compensation point, the effect of meteorological factors (temperature, wind speed, solar radiation, relative humidity, and precipitation) are represented, furthermore, it accounts for the total ammoniacal nitrogen ($TAN = NH_4^+ + NH_{3(aq)}$) budget on the surface simulating the conversion of uric acid content of guano to ammoniacal nitrogen. In addition, it also calculates the water budget on the surface using the Pennman equation for evaporation.

Several attempts have been made to simulate $NH_3$ emission from urine patches as well as grazed fields. Laubach et al. (2012) published an $NH_3$ volatilization model from urine patches which was run in an "inverse" mode to calculate soil resistance, applying also a simple compensation point model. The equilibrium gaseous $NH_3$ concentration in the soil pores was considered as a compensation point, and three resistances (a soil, an aerodynamic, and a quasi-laminar resistance) were assumed between the soil and air concentration. Running the model in predictive mode, simulating $NH_3$
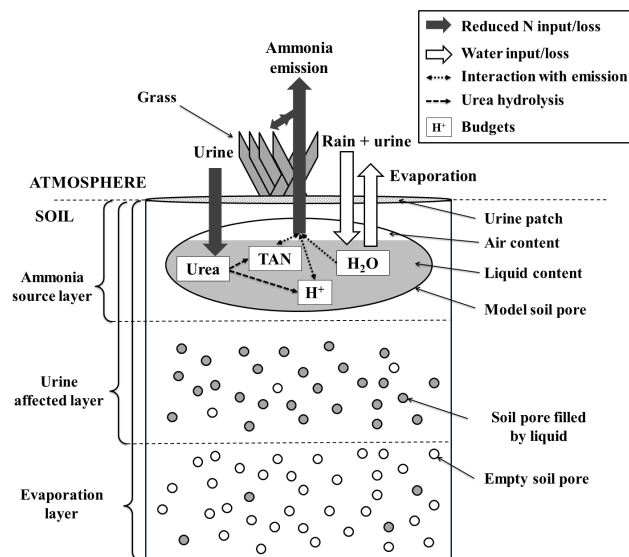


**Figure 1.** Schematic of major relationships in the GAG model. Empty soil pores in the middle layer represents that the maximum water content in the model is field capacity instead of being saturated. Whilst in the bottom layer the soil pores filled by liquid represents that the lowest water content is at the permanent wilting point instead of being completely dry. For more details on schematic see the text of Sect. 2.

emission, requires soil sampling and measurement of pH and $NH_4^+$ concentration of soil water.

The approach for the process of urea hydrolysis in the above-mentioned model by Laubach et al. (2012) is based on the earlier model of Sherlock and Goh (1985), which accounts for the $NH_3$ volatilization from urine patches and aqueous urea. This model for describing the transfer of $NH_3$ between surface and atmosphere operates with a constant "volatilization exchange coefficient", rather than a system of dynamically changing resistances. Rachhpal and Nye (1986) made an attempt to simulate $NH_3$ emission from applied urea. Although this model employed a constant "transfer coefficient" for $NH_3$ volatilization as well as a constant rate of urea hydrolysis were applied, the study gives an alternative for modelling the chemistry of a urine patch, as well as the vertical distribution of the different nitrogen compounds under the urine patch.

The present paper reports our work to construct and test a process-based, weather-driven model for $NH_3$ emission from a urine patch, which can be applied on both field and regional scales. On a field scale our approach is to apply the model for every urine patch deposited over the modelling period (involving statistical consideration), whilst for regional scale we are currently working to incorporate the field scale model into the EMEP4UK atmospheric chemistry transport model (Vieno et al., 2010, 2014). As such, the development represents a contribution toward developing a comprehensive suite of weather-dependent ammonia exchange models, as a

necessary basis for assessing the effects of climate change on ammonia emissions and deposition (Sutton et al., 2013). As soil measurements are not widely available – especially for a high-resolution grid that would be required for regional scale application – we had to account for the relevant processes in the soil, such as the change of concentration of the different reduced nitrogen compounds, pH, and water content. On the other hand, bearing in mind our final goal – a detailed investigation of weather dependency of $NH_3$ emission from grazing – we focused predominantly on the parametrization of the effect of meteorological variables, keeping the simulation of physical and chemical soil processes as simple as possible.

As our future aim is to apply the model to regional scale, simplicity to enhance scalability is a key aspect of the model development. For example, from a theoretical perspective, it could be attractive to explicitly model the 3-dimensional dispersion of ammonia between urine patches and adjacent vegetation within the canopy. However, this would be a much more complex task, which would also require major simplification when developing an upscaled regional application.

In this paper we firstly provide the description of our model of Generation of Ammonia from Grazing (GAG). Then we present the results from the test simulation based on the measurements by Laubach et al. (2012). Finally, we report the results of a sensitivity analysis in relation to the uncertain model parameters as well as several meteorological variables.
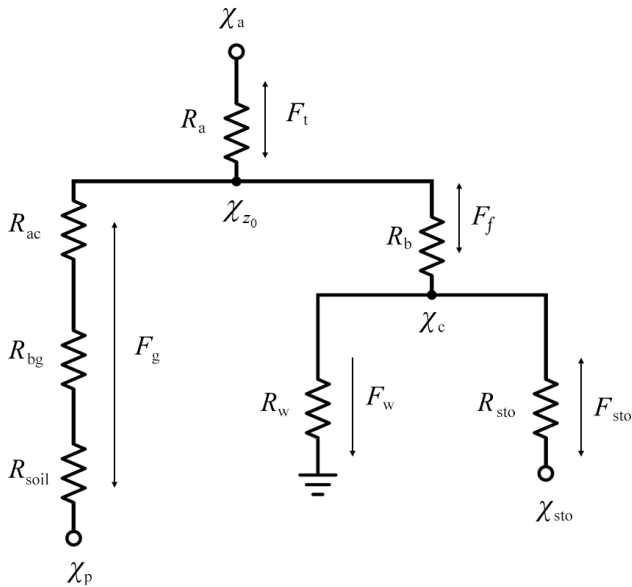
## 2 Description of the GAG model

To simulate $NH_3$ emission over a urine patch the GAG model calculates the TAN budget and the water budget, as well as the soil pH (hydrogen ion, $H^+$, budget) under the patch. For this purpose, firstly, we assume that, during urination and rain events, the incoming liquid infiltrates the soil to fill soil pores until the wetted soil layer reaches its field capacity. After this point we neglect any further downward or upward motion (capillary rise) in the soil. On Fig. 1 this depth in the soil is the bottom of the layer referred to as "urine affected layer".

We also make the assumption that soil $NH_3$ emission occurs only from the "source layer", the very top layer of the wetted soil column (similarly to Riedo et al., 2002, who also assumed a source layer on the top of their multilayer system), while reduced nitrogen (here the sum of $NH_x$ and urea) that infiltrates beneath this layer is assumed to be nitrified "and no longer available to $NH_3$ emission. This assumption allows us to handle the numerous soil pores in the source layer as a single big pore – referred hereafter as "model soil pore" – the liquid content of which represents the soil pores filled by liquid, while its gaseous section represents the air-filled soil pores in the source layer (Fig. 1). We assume that all the liquid content is at the bottom of the model soil pore and/or source layer.
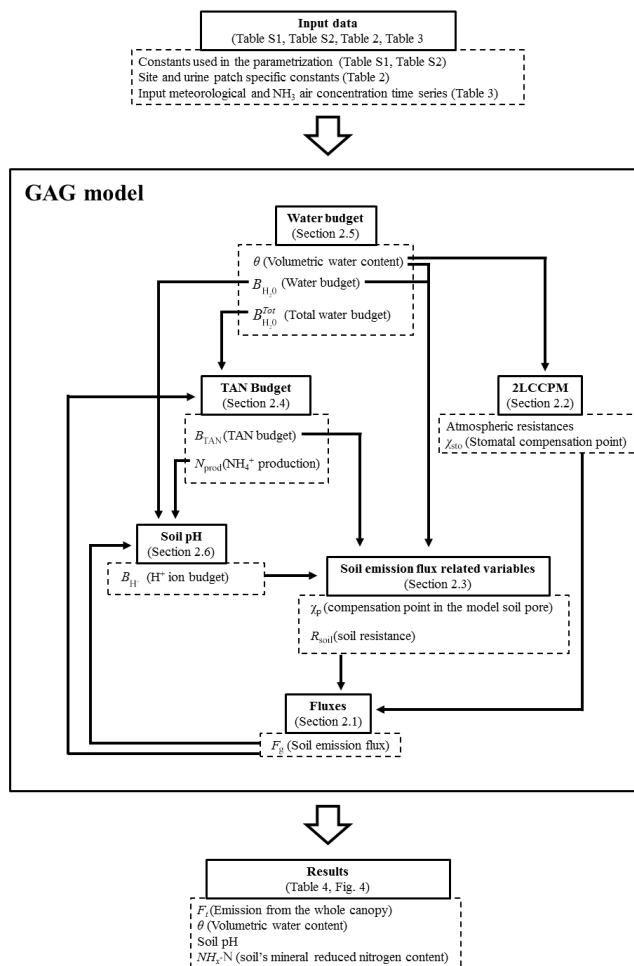


**Figure 2.** A flowchart depicting the steps of the calculation in the GAG model (middle panel), processing the input data (top panel) to the results that were compared with measurements in this study (bottom panel). The figure indicates the key variables that are carried from one module to another module(s). The figure, table, and section numbers referred in the figure show where further description of the different model parts can be found in this paper. (2LC-CPM stands for Two-Layer Canopy Compensation Point Model.)

The input to the TAN budget is generated by hydrolysis of the urea contained within incoming urine, while $NH_3$ emission acts as a loss from the TAN budget. Soil pH is also regulated by urea hydrolysis, which is a proton ($H^+$) consuming process, and by $NH_3$ emission which is a proton producing process. The water budget is increased by rain water and the liquid content of urine, whilst it is decreased by soil evaporation. We assume that water evaporates from the "evaporation layer" (as defined by Allen et al. (1998), see in more details in Sect. 2.5), and the soil dries from the top, that is, during evaporation a dry front moves downwards in the soil. The model was coded in R, version 3.1.2 (31 October 2014; R Core Team, 2012) and the steps of the calculation are shown in Fig. 2.

**Figure 3.** The network of gaseous resistances ($R$), ammonia concentrations ($\chi$), and ammonia fluxes ($F$) used in the GAG model, which is based on the two-layer canopy compensation point model of Nemitz et al. (2001) incorporating concentration of the soil pore ($\chi_p$) and soil resistance ($R_{soil}$). For the description of the other parameters in the framework see the text of this section.

## 2.1 Simulation of ammonia exchange flux

As urine deposition by grazing animals typically happens on vegetated surfaces of grassland we need to take into account the effect of vegetation on the total net $NH_3$ flux ($F_t$, calculated as emission minus deposition) over a urine patch. Therefore, an ideal model should capture not just the ground flux at the soil surface ($F_g$; referred hereafter as "soil emission"), but also the exchange with foliage ($F_f$), including $NH_3$ deposition to water and waxes on the leaf surface ($F_w$) and the $NH_3$ exchange with stomata ($F_{sto}$).

To achieve this, we extended the framework of the two-layer canopy compensation point model (abbreviated in this paper to 2LCCPM) of Nemitz et al. (2001) as shown in Fig. 3. The original exchange model calculates $F_g$ assuming a bulk soil compensation point on the soil surface. Instead of calculating this compensation point, we derive the compensation point for our model soil pore ($\chi_p$). To capture the constraint due to soil particles on $NH_3$ exchange with the soil, we added a soil resistance ($R_{soil}$) to the original framework.

Based on the analogy of electrical circuit, seven equations (Eqs. 1–7) can be derived to determine the five unknown fluxes ($F_t$, $F_g$, $F_f$, $F_w$, $F_{sto}$) and the two unknown compensation points (over the vegetation, $\chi_c$, and over the whole canopy, $\chi_{z0}$). Parameterizing the resistances – aerodynamic ($R_a$) and quasi-laminar resistance ($R_b$) over the canopy, aerodynamic resistance within the canopy ($R_{ac}$), quasi-laminar resistance ($R_{bg}$) at the ground, soil resistance, resistance to

water and wax on the leaf surface ($R_w$) and stomatal resistance ($R_{sto}$) – as well as calculating the compensation point in the soil pore and in the stomata ($\chi_{sto}$), we get a solvable linear system of equations.

$$F_t = F_g + F_f \tag{1}$$

$$F_f = F_w + F_{sto} \tag{2}$$

$$F_t = \frac{\chi_{z0} - \chi_a}{R_a} \tag{3}$$

$$F_g = \frac{\chi_p - \chi_{z0}}{R_{ac} + R_{bg} + R_{soil}} \tag{4}$$

$$F_f = \frac{\chi_c - \chi_{z0}}{R_b} \tag{5}$$

$$F_w = \frac{-\chi_c}{R_w} \tag{6}$$

$$F_{sto} = \frac{\chi_{sto} - \chi_c}{R_{sto}} \tag{7}$$

Assuming that the changes are close to linear within a time step (1 h), and taking the air concentration of ammonia high above the canopy ($\chi_a$) from measurements, the system of equations was solved for every time step by using the solve function of R programming language.

## 2.2 Parametrization of the resistances and stomatal compensation point ($R_a$, $R_b$, $R_{ac}$, $R_{bg}$, $R_w$, $R_{sto}$, $\chi_{sto}$)

The detailed parametrization of the resistances and the stomatal compensation point can be found in Sect. S1 in the Supplement together with all the model constants (Table S1 in the Supplement). Here we focus on the modifications and model assumptions we made for applying the 2LCCPM of Nemitz et al. (2001) in the GAG model.

Atmospheric resistances ($R_a$, $R_b$, $R_{ac}$, $R_{bg}$) are usually derived for homogenous (virtually infinite) surfaces, which is in apparent contradiction with the current application for a single, finite urine patch. In ongoing and future work we will apply the GAG model to field and regional scales, where the meteorological measurements and the canopy specific parameters, required to calculate these resistances, can be obtained for overall canopy types. To apply atmospheric resistances to urine patches, we assume that all the required variables and parameters to calculate them are representative for the whole experimental site including every single urine patch on the field (we also compared the results from GAG with measurements from a field experiment, as detailed in Sect. 4).

In the original description of the 2LCCPM, Nemitz et al. gave a parametrization for $R_a$ as a function of $u_*$ (friction velocity) and $L$ (Monin-Obukhov length), which were measured in the original modelling study. In the absence of measurements to obtain $u_*$ and $L$, parametrization should be used (Eqs. S7 and S8 in the Supplement, respectively). As these

two parameters depend on each other, we applied iteration to calculate both. For $R_b$ we applied the formula suggested by Nemitz et al., expressed by Eq. (S12).

Following Nemitz et al., $R_{ac}$ was assumed to be inversely proportional to $u_*$ ($R_{ac} = \alpha u_*^{-1}$). Massad et al. (2010b) recommended values for parameter $\alpha$ for many surface types – including grass – as well as for all of the four seasons (Table S1). Nemitz et al. applied a parametrization for $R_{bg}$ ($s\,m^{-1}$) for oilseed rape (Eq. S13). As the approach for calculation of this resistance for grasslands is not widely discussed in the literature, we adapted the one for oilseed rape for grassland. In our model, soil emission is dependent also on $R_{soil}$, which is larger at least by one order of magnitude than any of the atmospheric resistances. Thus, our model is not highly sensitive to this approximation for $R_{bg}$ (for detailed analysis of the model sensitivity see Sect. 5).

The cuticular exchange of ammonia is strongly linked to the presence of a water film on the waxy leaf surface (Flechard et al., 1999). This can form even below the saturation point for pure water vapour, as a result of condensation facilitated by hygroscopic particles on the plant surface (Burkhardt et al., 1999). Therefore, the cuticular resistance ($R_w$) describes the effect of this water film on $NH_3$ absorption. The extent to which such a thin water layer is present affects the value of $R_w$; however, $NH_3$ absorption is also dependent on the air concentration of the acidic components (especially $SO_2$). These compounds, decreasing the pH of the water film, favour $NH_3$ deposition (Flechard et al., 1999). The process is referred to as co-deposition of the different components.

The modelling of this phenomenon requires the knowledge of the chemical composition of the atmosphere and substantially increases model complexity. For a simpler approach, $R_w$ ($s\,m^{-1}$, Eq. 8) can be estimated as a function of relative humidity (RH, %). For this purpose – similarly also to Nemitz et al. (2001) – we used the formula from Massad et al. (2010b) based on Sutton and Fowler (1993) with the recommended parameters in the same study ($R_{w(min)}$ minimal cuticular resistance and $a$ for grassland as reported by Horváth et al., 2005):

$$R_w = R_{w(min)} \times \exp\left(a\left(100 - RH\right)\right). \tag{8}$$

In the original description of the 2LCCPM $R_{sto}$ is parametrized based on Hicks et al. (1987). Instead of this, we used a more state-of-the-art approach. As in Massad et al. (2010b), the value of $R_{sto}$ ($s\,m^{-1}$, Eq. 9) was derived from the stomatal resistance to ozone ($R_{sto}\,(O_3)$, $s\,m^{-1}$), taking into account the difference between the diffusivity of the two gases ($D_{O_3}/D_{NH_3} = 1/1.6$). On the other hand, in Eq. (10), we parametrized $R_{sto}$ (where 41 000 is the conversion from mmol $O_3\,m^{-2}$ to $m\,s^{-1}$) based on LAI (values are recommended by Massad et al. (2010b) for grass if not measured) applying the stomatal conductance ($g_s$, mmol $O_3\,m^{-2}$) model of Emberson et al. (2000).

$$R_{sto} = R_{sto}\,(O_3) \times \frac{D_{O_3}}{D_{NH_3}} \tag{9}$$

$$R_{sto}\,(O_3) = \left(\frac{g_s \times LAI}{41\,000}\right)^{-1} \tag{10}$$

Stomatal conductance Eq. (11) is defined based on the relative conductances that express how the openness of the stomata changes in the function of the phenological state of the plant ($g_{pot}$; assuming that grass could grow equally over the year, $g_{pot} = 1$), light ($g_{light}$), temperature ($g_{temp}$), vapour pressure deficit ($g_{VPD}$) and soil water potential ($g_{SWP}$). The combined effect of these, through the openness of stomata, controls $g_s$ between its maximal value ($g_{max}$) and its minimal value ($g_{max} \times g_{min}$):

$$g_s = g_{max}\, g_{pot}\max\left\{g_{min}, \left(g_{light}\, g_{temp}\, g_{VPD}\, g_{SWP}\right)\right\}. \tag{11}$$

We followed the suggested parametrization by Emberson et al. for $g_{light}$, $g_{temp}$, and $g_{VPD}$ (see in Sect. S1), but applied a different approach for $g_{SWP}$ (Eq. 12). As the GAG model simulates the volumetric water content of the soil ($\theta$, $m^3\,m^{-3}$; see the formulation in Sect. 2.5) for estimating $g_{SWP}$ – instead of using the original parametrization depending on the soil water potential – we adapted the approach by Simpson et al. (2012), who defined a soil moisture index ($S_{MI}$ Eq. 13), based on $\theta$, influenced also by the soil's permanent wilting point ($\theta_{pwp}$) and field capacity ($\theta_{fc}$).

$$g_{SWP} = \begin{cases} 1 & \text{if} & S_{MI} \geq 0.5 \\ 2 \times S_{MI} & \text{if} & S_{MI} < 0.5 \end{cases} \tag{12}$$

$$S_{MI} = \frac{\theta - \theta_{pwp}}{\theta_{fc} - \theta_{pwp}} \tag{13}$$

The stomatal compensation point, as the equilibrium gaseous $NH_3$ concentration in the stomata, can be derived from the temperature-dependent form of Henry's law for dissolution of $NH_3$ (Reaction (R1) in Table 1) and the dissociation coefficient of $NH_4^+$ (Reaction (R4) in Table 1). Nemitz et al. (2000) derived $\chi_{sto}$ (Eq. 14) as a function of temperature (K) and the emission potential of the stomata ($\Gamma_{sto}$), which equals to the ratio of the $NH_4^+$ and $H^+$ concentrations (mol $dm^{-3}$) in the apoplastic fluid in the stomatal cavity.

$$\chi_{sto} = \frac{161\,500}{T} \times \exp\left(\frac{-10\,380}{T}\right) \times \Gamma_{sto} \tag{14}$$

In the original 2LCCPM $\Gamma_{sto}$ is an input parameter from measurements. Since the measurement of $\Gamma_{sto}$ is very difficult, in models it is usually handled as a constant, parametrized or simulated by a sub-model (e.g. Massad et al., 2010a; Wu et al., 2009). As there were no $\Gamma$ measurements

**Table 1.** Chemical equations – indicated by Reactions (R0)–(R5) – simulated within the model, (where applicable) their equilibrium coefficient according to definition ($K$ for dissociation and H for dissolution) and the coefficients expressed as the function of soil temperature ($T_{soil}$, $K$) and their references (squared brackets denotes that the concentration of every compound is in $mol\,dm^{-3}$).

| Chemical equation | Equilibrium coefficient | Equilibrium coefficient as a function of temperature | Reference |
|---|---|---|---|
| R0: $CO(NH_2)_2 + 2H_2O + H^+ \rightarrow 2NH_4^+ + HCO_3^-$ | – | – | – |
| R1: $NH_4^+ \Leftrightarrow NH_{3(aq)} + H^+$ | $K\left(NH_4^+\right) = \frac{[NH_{3(aq)}][H^+]}{[NH_4^+]}$ | $K\left(NH_4^+\right) = 5.67 \times 10^{-10} \exp\left(-6286\left(\frac{1}{T_{soil}} - \frac{1}{298.15}\right)\right)$ | Bates and Pinching (1949) |
| R2: $HCO_3^- \Leftrightarrow CO_3^{2-} + H^+$ | $K\left(HCO_3^-\right) = \frac{[H^+][CO_3^{2-}]}{[HCO_3^-]}$ | $a = 2902.39$ $b = 0.02379$ $c = 6.4980$ | Harned and Scholes (1941) |
| R3: $H_2CO_3 \Leftrightarrow HCO_3^- + H^+$ | $K(H_2CO_3) = \frac{[HCO_3^-][H^+]}{[H_2CO_3]}$ | $\lg(K(X)) = -\left(\left(\frac{a}{T_{soil}}\right) + (b \times T_{soil}) - c\right)$ $a = 3404.71$ $b = 0.032786$ $c = 14.8435$ | Harned and Davis (1943) |
| R4: $NH_{3(aq)} \Leftrightarrow NH_{3(g)}$ | $H\left(NH_{3(g)}\right) = \frac{[NH_{3(aq)}]}{[NH_{3(g)}]}$ | $H\left(NH_{3(g)}\right) = 56 \times \exp\left(4092 \times \left(\frac{1}{T_{soil}} - \frac{1}{298.15}\right)\right) \times c_{con}$ | Dasgupta and Dong (1986) |
| R5: $H_2CO_3 \Leftrightarrow CO_{2(g)}$ | $H\left(CO_{2(g)}\right) = \frac{[H_2CO_3]}{[CO_{2(g)}]}$ | $H\left(CO_{2(g)}\right) = 0.034 \times \exp\left(2400 \times \left(\frac{1}{T_{soil}} - \frac{1}{298.15}\right)\right) \times c_{con}$ | Wilhelm et al. (1977) |

where $c_{con} = \left(\frac{0.001\frac{m^3}{dm^3}}{8.314\frac{J}{K\,mol}} \times \frac{1.013 \times 10^5\frac{Pa}{atm}}{T_{soil}}\right)^{-1}$ is the conversion from atm $(mol\,dm^{-3})^{-1}$ to $(mol\,dm^{-3})(mol\,dm^{-3})^{-1}$

in the experiment we used in the test simulation (nor would such measurements be available for regional scale application) and over a urine patch $NH_3$ exchange is dominated by soil emission, we chose the parametrization recommended by Massad et al. (2010b) for grazed fields. Equation (15) assumes that $\Gamma_{sto}$ reaches its maximum $\Gamma_{sto}$ (max) right after N application (in this case after urine deposition), and then decays exponentially with time ($t_i$ indicates the time step, the hours spent after urine deposition, with a decay parameter $\tau$ set at $2.88 \times 24\,h$).

$$\Gamma_{sto}(t_i) = \Gamma_{sto}(max) \times \exp\left(-\frac{t_i - 1}{\tau}\right) \qquad (15)$$

Massad et al. (2010b) proposed a parametrization, describing an empirical relationship (Eq. 16) between the total N applied to the ecosystem ($N_{app}$ in $kg\,N\,ha^{-1}$, see Eq. 17) and the observed maximal stomatal $NH_3$ emission potential ($\Gamma_{sto}$ (max)). To apply the formula for a urine patch, we calculated $N_{app}$ as the total N content of the urine – the volume of urine ($W_{urine}$, $dm^3$) multiplied by its nitrogen content ($c_N$, $gN\,dm^{-3}$) – divided by the area of the urine patch ($A_{patch}$, $m^2$; with 10 as a conversion factor between the different units).

$$\Gamma_{sto}(max) = 12.3 \times N_{app} + 20.3 \qquad (16)$$

$$N_{app} = \frac{W_{urine} \times c_N}{A_{patch}} \times 10 \qquad (17)$$

## 2.3 Simulation of the soil pore ($\chi_p$) compensation point and the soil resistance ($R_{soil}$)

The simulation of $\chi_p$ ($mol\,dm^{-3}$) is very similar in theory to that of $\chi_{sto}$, being derived from Henry's law for $NH_3$ dissolution and the dissociation coefficient of $NH_4^+$. In this way

(following Nemitz et al., 2000) we get Eq. (18), where $T_{soil}$ is the soil temperature ($K$) and $\Gamma_p$ is the ratio of the $NH_4^+$ and $H^+$ concentration in the model soil pore. In Eq. (19) $\Gamma_p$ is expressed as a function of TAN concentration ($[TAN] = [NH_4^+] + [NH_{3(aq)}]$) based on the definition of dissociation constant ($K(NH_4^+)$, second column of Table 1 and its temperature-dependent form in the third column).

$$\chi_p = \frac{161\,500}{T_{soil}} \times \exp\left(\frac{-10\,380}{T_{soil}}\right) \times \Gamma_p \qquad (18)$$

$$\Gamma_p = \frac{[TAN]}{K\left(NH_4^+\right) + [H^+]} \qquad (19)$$

TAN and $H^+$ concentration (both in $mol\,dm^{-3}$) are derived from TAN budget ($B_{TAN}$, g N) and $H^+$ budget ($B_{H+}$, mol), according to their mass ratio with water budget ($B_{H_2O}$, $dm^3$), as shown in Eqs. (20)–(21), respectively, (where 14 is the molar mass of nitrogen). All budgets are simulated within GAG (see $B_{TAN}$: Sect. 2.4, $B_{H+}$: Sect. 2.6, and $B_{H_2O}$: Sect. 2.5).

$$[TAN] = \frac{\frac{B_{TAN}}{14}}{B_{H_2O}} \qquad (20)$$

$$[H^+] = \frac{B_{H+}}{B_{H_2O}} \qquad (21)$$

For $R_{soil}$ ($s\,m^{-1}$) we applied the approach by Laubach et al. (2012), as expressed in Eq. (22). This captures the effect of soil depth ($\Delta z$), that is, from how deep the soil $NH_3$ emission occurs on average. In the study of Laubach et al. $\Delta z$ is referred as "source depth", and in GAG model we consider it as the thickness of the source layer. The model experiments by Laubach et al. suggested that the distribution of $\Delta z$ has a median of $0.002\,m$ with an uncertainty factor of 2

and a similar value (0.003 m) was used in the study of Riedo et al. (2002) as well. In reality the thickness of the source layer changes parallel with the moisture content of the top soil layer; however, its approximation, due to the thinness of the layer, is difficult. Therefore, at the moment our model operates with a constant $\Delta z$ of 0.004 m. In Sect. 5.2 we tested the model sensitivity also to $\Delta z$.

$$R_{\text{soil}} = \frac{\Delta z}{\xi D_{\text{g}}} \tag{22}$$

According to this approach, $R_{\text{soil}}$ is inversely proportional to soil tortuosity ($\xi$) and diffusivity of $NH_3$ ($D_{\text{g}}$). For $\xi$, Laubach et al. (2012) suggested the parametrization by Millington and Quirk (1961), based on the volumetric water content as well as porosity ($\theta_{\text{por}}$):

$$\xi = \frac{\left(\theta_{\text{por}} - \theta\right)^{\frac{10}{3}}}{\theta_{\text{por}}^2}. \tag{23}$$

## 2.4 Simulation of the TAN budget under the urine patch ($B_{\text{TAN}}$)

The amount of TAN in the model soil pore in a given time step $t_i$ ($B_{\text{TAN}}(t_i)$, g N), depends on its value in the previous time step ($B_{\text{TAN}}(t_{i-1})$, g N) and is controlled by the amount of TAN produced during urea hydrolysis ($N_{\text{prod}}$, g N) and soil $NH_3$ emission ($F_{\text{g}}$, g N m$^{-2}$) calculated in the previous time step (Eq. 24). We assume that $B_{\text{TAN}}$ before urine deposition is negligibly small (compared to that of after urine deposition). Therefore, its initial value is set to 0. The model does not allow to emit more $NH_3$ than TAN is available in the source layer, as it is described by Eq. (25).

$$B_{\text{TAN}}(t_i) = N_{\text{prod}}(t_i) + B_{\text{TAN}}(t_{i-1}) - F_{\text{g}}(t_{i-1}) \times A_{\text{patch}} \tag{24}$$

$$F_{\text{g}} = \begin{cases} \dfrac{B_{\text{TAN}}(t_{i-1})}{A_{\text{patch}}} & \text{if}\left(B_{\text{TAN}}(t_{i-1}) - F_{\text{g}}(t_{i-1}) \times A_{\text{patch}}\right) < 0 \\ \dfrac{\chi_{\text{p}} - \chi_{z_0}}{R_{\text{ac}} + R_{\text{bg}} + R_{\text{soil}}} & \text{otherwise} \end{cases} \tag{25}$$

TAN production depends on the current amount of urea nitrogen within the model soil pore ($B_{\text{urea}}$, g N), as well as soil temperature ($T_{\text{soil}}$, °C). For $N_{\text{prod}}$ Sherlock and Goh (1985) suggested an empirical formula (Eq. 26), with a temperature-dependent parameter ($A_{\text{h}}$, Eq. 27) and a hydrolysis constant ($k_{\text{h}}$, see Table 2).

$$N_{\text{prod}}(t_i) = B_{\text{urea}}(t_i)\left(1 - \exp\left(A_{\text{h}}(t_i) \times k_{\text{h}}\right)\right) \tag{26}$$

$$A_{\text{h}}(t_i) = 0.25 \times \exp\left(0.0693 \times T_{\text{soil}}(t_i)\right) \tag{27}$$

**Table 2.** Urine patch details from the experiment of Laubach et al. (2012) or from other sources as listed in the footnote and site specific model constants.

| Model constants | Value |
|---|---|
| Urine patch specific constants | |
| $A_{\text{patch}}$ (area of a urine patch)[1] | 0.25 m$^2$ |
| $c_{\text{N}}$ (N content of the urine) | 10 g N dm$^{-3}$ |
| $W_{\text{urine}}$ (volume of urine) | 1.5 dm$^3$ |
| $\Delta z$ (thickness of the source layer)[2] | 4 mm |
| $k_{\text{h}}$ (urea hydrolysis constant)[3] | 0.23 |
| Site specific constants | |
| Longitude | 172°27.34′ E |
| Latitude | 43°38.56′ S |
| Height above sea level | 11 m |
| $\theta_{\text{pwp}}$ (permanent wilting point)[4] | 0.1 |
| $\theta_{\text{fc}}$ (field capacity)[4] | 0.4 |
| $\theta_{\text{por}}$ (porosity) | 0.62 |
| $f_{\text{c}}$ (vegetation coverage) | 35 % |
| $z_{\text{w}}$ (height of wind measurement) | 2.1 m |

[1] In the experiment the expansion of the patches was observed up to 0.5 m$^2$. For model sensitivity to $A_{\text{patch}}$ see Sect. 5.2. [2] Assumed in this study. [3] For summer (Sherlock and Goh, 1984) [4] Assumed based on the provided measured volumetric water content data set.

Urea nitrogen content in a given time step (Eq. 28) is determined by its value in the previous time step, the loss as conversion to TAN ($-N_{\text{prod}}$) and, in the first time step, the amount of urea nitrogen added ($U_{\text{add}}$, g N) with the incoming urine. In $U_{\text{add}}$ (Eq. 29) we take into account the dilution effect of rain and soil water on the nitrogen concentration of urine ($c_{\text{n}}$). We assume that right after urine deposition the urea nitrogen content of urine, diluting in the total soil water ($B_{\text{H}_2\text{O}}^{\text{Tot}}$, Eq. 29), forms a homogenous soil solution with a concentration of $c_{\text{n}}^{\text{Tot}}$ (Eq. 30). Finally, $U_{\text{add}}$ is calculated as the product of $c_{\text{n}}^{\text{Tot}}$ and the water content of the emission layer. This will equal to $B_{\text{H}_2\text{O}}^{\text{Tot}}$ unless there is more water in the soil than can be stored in the emission layer, as indicated by $B_{\text{H}_2\text{O}}$ (max), which is specified in the following section, see Eq. (36).

$$B_{\text{urea}}(t_i) = B_{\text{urea}}(t_{i-1}) - N_{\text{prod}}(t_{i-1}) + U_{\text{add}}(t_i) \tag{28}$$

$$U_{\text{add}} = c_{\text{n}}^{\text{Tot}} \min\left\{B_{\text{H}_2\text{O}}(\text{max}), B_{\text{H}_2\text{O}}^{\text{Tot}}\right\} \tag{29}$$

$$c_{\text{n}}^{\text{Tot}} = c_{\text{n}} \frac{W_{\text{urine}}}{B_{\text{H}_2\text{O}}^{\text{Tot}}} \tag{30}$$

## 2.5 Simulation of the water budget under the urine patch ($B_{\text{H}_2\text{O}}^{\text{Tot}}$, $\theta$, $B_{\text{H}_2\text{O}}$, $B_{\text{H}_2\text{O}}(\text{max})$)

The soil moisture content affects $NH_3$ emission in several ways. In the first time step when the urine is deposited, both the water content of the model soil pore and the water content

of the whole urine-affected soil layer ($B_{H_2O}^{Tot}$, Eq. 31) have an effect on emission. The thickness of the urine-affected soil layer depends on the amount of incoming liquids: urine (considering its whole volume as water) and rain ($W_{rain}$, dm$^3$). The more water is added, the more empty soil pore it can fill up and consequently, the deeper it will infiltrate.

We made the assumption for our model that the lowest possible volumetric water content in the soil is at permanent wilting point ($\theta_{pwp}$) and the highest is at the field capacity ($\theta_{fc}$), where both $\theta_{pwp}$ and $\theta_{fc}$ are expressed as fractions of total soil volume. Assuming that the initial soil water content is at $\theta_{pwp}$, and after infiltration it rises to $\theta_{fc}$, the volume fraction taken up by the incoming water will be $\theta_{fc} - \theta_{pwp}$. Finally, we get the total water content (incoming + soil water) in the urine-affected layer (having a volumetric water content of $\theta_{fc}$) as

$$B_{H_2O}^{Tot} = (W_{rain}(t_1) + W_{urine}) \frac{\theta_{fc}}{\theta_{fc} - \theta_{pwp}}. \tag{31}$$

After urine deposition, actual volumetric water content ($\theta$, Eq. 32) of the source layer can be expressed as the volume of the water in the layer ($B_{H_2O}$, dm$^3$) divided by the volume of the soil column under the urine patch with a surface area of $A_{patch}$ (m$^2$). In Eq. (32) 1000 is the conversion from m$^3$ to dm$^3$).

$$\theta = \frac{B_{H_2O}}{1000 \times \Delta z \times A_{patch}} \tag{32}$$

The actual water content of the soil at any time step ($B_{H_2O}'(t_i)$, Eq. 33) depends on the water content in the previous time step, soil evaporation ($W_{evap}$, dm$^3$), rain events ($W_{rain}$, dm$^3$), and in the very first time step the volume of urine (e.g. if the volume of the urine is 1.5 dm$^3$ then $W_{urine}$ ($t_1$) = 1.5 dm$^3$, otherwise 0). Both the volume of evaporation from the source layer and incoming rain to this layer are derived as the product of $A_{patch}$ and soil evaporation (with $E$ (dm$^3$ m$^{-2}$): $W_{evap} = E \times A_{patch}$) as well as precipitation (with $P$ (dm$^3$ m$^{-2}$): $W_{rain} = P \times A_{patch}$) for a m$^2$, respectively.

$$B_{H_2O}'(t_i) =$$
$$\begin{cases} B_{H_2O}(min) + W_{rain}(t_i) + W_{urine}(t_i) \\ \quad \text{if } (B_{H_2O}(t_{i-1}) - W_{evap}(t_{i-1})) < B_{H_2O}(min) \\ B_{H_2O}(t_{i-1}) - W_{evap}(t_{i-1}) + W_{rain}(t_i) + \quad \text{otherwise} \\ \quad W_{urine}(t_i) \end{cases}$$
$$\tag{33}$$

It is not possible for more water to be evaporated from the source layer than the minimal water content (water content of the layer at $\theta_{pwp}$: $B_{H_2O}(min)$ (dm$^3$), Eq. 34). On the other hand, (as is shown in Eq. 35) this layer cannot store more

water than the maximal water content (water content of the layer at $\theta_{fc}$: $B_{H_2O}(max)$ (dm$^3$), Eq. 36). The excess water is assumed to infiltrate to the deeper soil layers. In Eqs. (34) and (36) 1000 is the conversion from m$^3$ to dm$^3$.

$$B_{H_2O}(min) = 1000 \times \Delta z \times A_{patch} \times \theta_{pwp} \tag{34}$$

$$B_{H_2O}(t_i) = min\{B_{H_2O}'(t_i), B_{H_2O}(max)\} \tag{35}$$

$$B_{H_2O}(max) = 1000 \times \Delta z \times A_{patch} \times \theta_{fc} \tag{36}$$

Instead of constructing a comprehensive energy balance model for GAG (driving NH$_3$ and water vapour flux in the same time), for simplicity's sake, to estimate the soil evaporation we adapted the dual crop method of Allen et al. (1998). The approach firstly calculates the reference evapotranspiration (ET$_0$, evaporation from soil + transpiration by plants) for a reference surface (a surface covered by grass with a height of 0.12 m, a fixed surface resistance to water exchange of 70 s m$^{-1}$ and albedo of 0.23). Then, defining a "crop coefficient" ($K_c$) for the actual surface, it gives an estimation for the actual evapotranspiration (ET = $K_c \times$ ET$_0$). In the final step $K_c$ is split to a coefficient for transpiration and a coefficient for soil evaporation ($K_c = K_{cb} + K_e$).

In our model for ET$_0$ we incorporated a slightly modified form of the Penman-Monteith equation (Eq. (37), Walter et al., 2001) compared with that of Allen et al. (1998). In this way the model accounts for the effect of change of day and night on evapotranspiration ($C_d$, Eq. 38). For the formulation of $\Delta$ (the slope of the saturation vapour pressure temperature relationship), $R_n$ (net radiation), $G$ (soil heat flux) and $\gamma$ (psychrometric constant), see the details in Allen et al. (1998).

$$ET_0 = \frac{0.408 \times \Delta (R_n - G) + \gamma \frac{37}{T + 273.15} u (e_s - e_a)}{\Delta + \gamma (1 + C_d u)} \tag{37}$$

$$C_d = \begin{cases} 0.24 & \text{if} \quad R_n > 0 \quad \text{(daytime)} \\ 0.96 & \text{otherwise} \quad \text{(nighttime)} \end{cases} \tag{38}$$

When calculating soil evaporation ($E = K_e \times$ ET$_0$) we made the following assumptions:

- According to Allen et al., soil evaporation occurs from the wetted, uncovered soil fraction ($f_w$). Applying the evapotranspiration model for a urine patch, the whole modelled soil will be wet. In addition, we assumed that the percentage of the whole field covered by vegetation ($f_c$) is the same over a urine patch. In this way $f_w = (1 - f_c)$ for a urine patch.

- Following the recommendations of Allen et al., we assumed that there is no runoff, no transpiration from the evaporation layer (including the NH$_3$ source layer) and no "deep percolation" (which occurs when $\theta$ exceeds $\theta_{fc}$, but in our model $\theta_{fc}$ is assumed to be the maximum of $\theta$).

– In the original approach it is assumed that soil evaporation attenuates when more water is evaporated from the soil evaporation layer (characterized by a thickness of $\Delta z_E$) than the amount of "readily evaporable water" (REW). The study of Allen et al. recommends REW values for different soil types defined by their $\theta_{fc}$ and $\theta_{pwp}$. However, for the site whose measurement we used in the test simulation (see Sect. 4.), with a sandy loam soil, these $\theta_{fc}$ and $\theta_{pwp}$ values were not in accordance with the measurements. Therefore, we calculated REW as the water content of the evaporation layer halfway between $\theta_{fc}$ and $\theta_{pwp}$:

$$\text{REW} = 1000 \left( \theta_{fc} - 0.5 \left( \theta_{fc} - \theta_{pwp} \right) \right) \times \Delta z_E. \qquad (39)$$

The model constants used in the soil evaporation estimation are listed in Table S2.

## 2.6 Simulation of soil pH ($B_{H+}$)

After urine deposition, soil pH is affected by two main reactions: urea hydrolysis and $NH_3$ emission. When a urea molecule is decomposed (based on Reaction (R0) in Table 1) an $H^+$ ion is consumed, producing two $NH_4^+$ ions and a bicarbonate ion ($HCO_3^-$). In the early stages of urea hydrolysis, when a large amount of urea is hydrolysed, a large amount of $H^+$ is required, resulting in a peak of soil pH (minimum of soil $H^+$ concentration). This triggers the dissociation of the produced $NH_4^+$ and consequently the formation of gaseous ammonia, which also leads to an emission peak shortly after urine deposition. Once the majority of urea has been hydrolysed, ammonia emission may still be continuing. To balance the lost gaseous ammonia, more $NH_4^+$ dissociates, resulting in $H^+$ production, which tends to compensate the $H^+$ consumption associated with urea hydrolysis.

According to Sherlock and Goh (1985) after a rapid increase, soil pH usually peaks around 6–48 h after urine deposition (referred to as "first stage" of emission). Subsequently, the pH tends to drop for the reasons explained above over a period of about 2–8 days (second stage). Sherlock and Goh also identified two further stages: a 1–3 week long constant phase (third stage) when soil pH does not change considerably and, finally, a phase (fourth stage) with a moderate decline in soil pH, regulated by the nitrification of TAN.

As Sherlock and Goh (1985) pointed out that the bulk of TAN is volatilized over the first and second periods, and nitrification is a sufficiently slower process than $NH_3$ volatilization (see the cited references in the study of Sherlock and Goh), in the GAG model we neglect the effect of nitrification. On the other hand, we make the assumption that the solid material of soil is chemically inert, and consequently, $NH_3$ emission from soil is only affected by the composition of urine solution.

Whitehead et al. (1989) showed that not only urea but other urinary nitrogen components, such as allantoin, creatine and creatinine, can contribute to $NH_3$ emission through their decomposition. However, Whitehead et al. found that only allantoin can have a comparable influence on $NH_3$ volatilization (from the solutions of these compounds with the same N concentration, over 8 days 15 % of the applied N was emitted from urea and 11 % from the allantoin); that of the other two components, creatine and creatinine, is rather small (over 8 days 4 % and less than 1 % of the applied N was emitted as $NH_3$, respectively). In addition, according to Dijkstra et al. (2013) the proportion of allantoin in urinary nitrogen is considerably lower than that of urea, 2.2–14.2 compared to 57.8–93.5 % and the proportions for creatine and creatinine are even lower. Therefore, to further focus our model onto the key reactions, we simulate urine chemistry considering only the water and urea available in the beginning, and the products of urea breakdown afterwards.

As urine is a relatively concentrated solution, non-ideal ionic behaviour may have an effect on the chemical equilibria. To test this in the model, we did a test run with the maximum activity coefficients derived for the highest ion concentrations (0.2 mol dm$^{-3}$) published by Kielland (1937; the highest ionic concentration in the modelled solution was 0.14 mol dm$^{-3}$). With this modification, the difference, in the total $NH_3$ emission was $-4.7$ % and the average change in pH was $-0.019$. Considering that the ion concentration decreases toward the end of the modelling period, and consequently, the activity coefficients converge to 1, we neglect the effect of non-ideal behaviour in the solution.

In this way, we consider the reactions for change of soil pH listed in Table 1: urea hydrolysis (Reaction R0), $NH_4^+$ dissociation (R1), dissociation of $HCO_3^-$ and $H_2CO_3$ (carbonic acid; Reactions (R2) and (R3), respectively), formation of gaseous $NH_3$ and $CO_2$ (carbon dioxide; Reactions (R4) and (R5), respectively). However, considering that soil is a buffered system, we also incorporate a soil buffering capacity ($\beta$ mol $H^+$ (pH unit)$^{-1}$ dm$^{-3}$). Buffering capacity moderates the change of $H^+$ ion concentration. When $H^+$ ions are produced in the system during urea hydrolysis and the related equilibrium processes, to balance this change $H^+$ ions are consumed by buffers, and similarly, when $H^+$ ions are consumed in the system, buffers release $H^+$ ions. In the model this buffering effect is expressed by the term of $\beta_{patch}$ (pH($t_i$)-pH($t_{i-1}$)) in Eq. (46). This term is positive when the $H^+$ ion concentration decreases (pH increases), and it is negative in the opposite case.

Whitehead and Raistrick (1993) found a strong correlation between the cation exchange capacity (CEC) and $NH_3$ volatilization as well as a weaker correlation with organic matter, clay, and sand content of the soil. However, we are not aware of a specific quantitative relationship between buffering capacity and CEC, or the clay content or the organic matter content. Therefore, we address this issue through a sensitivity analysis on the model performance (Sect. 5.3).

Regarding the effect of the potassium content of urine on buffering capacity and indirectly, $NH_3$ emission, Whitehead et al. (1989) showed that the potassium salts of urine have a rather small influence on $NH_3$ volatilization. Based on these, we used a constant buffering capacity in the model. We defined $\beta$ during test simulations with GAG. We found that the model represents the measured pH well with a $\beta$ of 0.021 mol $H^+$ (pH unit)$^{-1}$ dm$^{-3}$. To get the buffering effect in the volume of our model soil pore we calculated $\beta_{patch} = \beta \times A_{patch} \times \Delta z$. For a sensitivity analysis to $\beta$ see Sect. 5.3.

We defined 13 equations to calculate soil pH (Eqs. 40–52), eight of which are predictive equations, Eqs. (40)–(47), where $B_X$ (mol) is the budget of the component $X$ in the urine solution and $r_{Rx}$ (mol) is the production or consumption of the compound predicted by the given equation in the reaction $X$ (following the numbering of reactions in Table 1). Variables $i_N$ and $i_C$ indicate the nitrogen and carbon input generated during urea hydrolysis, respectively. The nitrogen input is the same as $N_{prod}$ but in mol ($i_N = N_{prod}/14$) and based on R0, $i_C = i_N/2$.

The other five equations describe the equilibrium in every time step (Eqs. 48–52). These were derived by reorganizing the equations in the second column in Table 1, where, for a dissolved component $X$: $[X] = B_x/B_{H_2O}$ and for a gaseous component $X_{(g)}$: $[X_{(g)}] = B_{X(g)}/V_{air}$. $V_{air}$ is the volume of the air in the model soil pore, which can be calculated as the volume of the space in the model soil pore that is not taken up by the liquid content ($V_{air} = \theta_{por} A_{patch} \Delta z \times 1000 - B_{H_2O}$, where 1000 is the conversion between m$^3$ and dm$^3$).

Variables $B_C$ and $B_N$ represent the total inorganic carbon and nitrogen budget in the urine solution, respectively. Both can be derived as a sum of the different components and their input (by urea breakdown) and loss via emission as gas (Eqs. 53 and 54).

$$B_{H_2CO_3}(t_i) = B_{H_2CO_3}(t_{i-1}) + (-r_{R5} + r_{R3}) \tag{40}$$

$$B_{HCO_3^-}(t_i) = B_{HCO_3^-}(t_{i-1}) + (-r_{R2} - r_{R3} + i_C(t_i)) \tag{41}$$

$$B_{CO_3^{2-}}(t_i) = B_{CO_3^{2-}}(t_{i-1}) + r_{R2} \tag{42}$$

$$B_{CO_2(g)}(t_i) = B_{CO_2(g)}(t_{i-1}) + r_{R5} \tag{43}$$

$$B_{NH_4^+}(t_i) = B_{NH_4^+}(t_{i-1}) + (-r_{R1} + i_N(t_i)) \tag{44}$$

$$B_{NH_3(aq)}(t_i) = B_{NH_3(aq)}(t_{i-1}) + (r_{R1} - r_{R4}) \tag{45}$$

$$B_{NH_3(g)}(t_i) = B_{NH_3(g)}(t_{i-1}) + \left(r_{R4} - \frac{F_g(t_{i-1}) \times A_{patch}}{14}\right) \tag{46}$$

$$B_{H^+}(t_i) = B_{H^+}(t_{i-1}) - i_C(t_i) + (-r_{R3} + r_{R2} + r_{R1}) + \beta_{patch}(\text{pH}(t_i) - \text{pH}(t_{i-1})) \tag{47}$$

$$K\left(NH_4^+\right)(t_i) B_{H_2O}(t_i) B_{NH_4^+}(t_i) - B_{H^+}(t_i) B_{NH_3(aq)}(t_i) = 0 \tag{48}$$

$$K\left(CO_3^-\right)(t_i) B_{H_2O}(t_i) B_{HCO_3^-}(t_i) - B_{H^+}(t_i) B_{CO_3^{2-}}(t_i) = 0 \tag{49}$$

$$K(H_2CO_3)(t_i) B_{H_2O}(t_i) B_{H_2CO_3}(t_i) - B_{H^+}(t_i) B_{HCO_3^-}(t_i) = 0 \tag{50}$$

$$\left(H\left(CO_{2(g)}\right)(t_i) \frac{B_{H_2O}(t_i)}{V_{air}(t_i)} + 1\right) B_{H_2CO_3}(t_i)$$
$$+ H\left(CO_{2(g)}\right)(t_i) \frac{B_{H_2O}(t_i)}{V_{air}(t_i)}$$
$$B_{HCO_3^-}(t_i) + H\left(CO_{2(g)}\right)(t_i) \frac{B_{H_2O}(t_i)}{V_{air}(t_i)} B_{CO_2}(t_i)$$
$$= H\left(CO_{2(g)}\right)(t_i) \frac{B_{H_2O}(t_i)}{V_{air}(t_i)} B_C(t_i) \tag{51}$$

$$\left(H\left(NH_{3(g)}\right)(t_i) \frac{B_{H_2O}(t_i)}{V_{air}(t_i)} + 1\right) B_{NH_3(aq)}(t_i)$$
$$+ H\left(NH_{3(g)}\right)(t_i) \frac{B_{H_2O}(t_i)}{V_{air}(t_i)} B_{NH_4^+}(t_i)$$
$$= H\left(NH_{3(g)}\right)(t_i) \frac{B_{H_2O}(t_i)}{V_{air}(t_i)} B_N(t_i) \tag{52}$$

$$B_C(t_i) = B_{H_2CO_3}(t_{i-1}) + B_{HCO_3^-}(t_{i-1}) + B_{CO_3^{2-}}(t_{i-1}) + B_{CO_2}(t_{i-1}) + i_C(t_i) \tag{53}$$

$$B_N(t_i) = B_{NH_3(aq)}(t_{i-1}) + B_{NH_4^+}(t_{i-1}) + B_{NH_3(g)}(t_{i-1}) + i_N(t_i) - \frac{F_g(t_{i-1}) \times A_{patch}}{14} \tag{54}$$

Although references can be found in the literature for measurements of $CO_2$ emission from urine patches (e.g. Wang et al., 2013; Ma et al., 2006; Lin et al., 2009), we considered that the driving processes behind them are not described well enough for an hourly model application. Therefore, in the case of the carbon budget (Eq. 53) we did not assume a term for $CO_2$ emission in the basic GAG model, but we tested the effect of $CO_2$ emission in Sect. 5.3. The dissociation coefficients ($K(X)(t_i)$) and Henry constants ($H(X(g))(t_i)$) for the given $t_i$ time step were derived as a function of actual soil temperature (third column of Table 1).

For a given $B_{H^+}(t_i)$ Eqs. (40)–(46) and (48)–(52) constitute a linear system of equations (12 equations, and seven $B_X(t_i)$ budgets and five $r_{Rx}$ consumptions and/or productions as unknowns). As $B_{H^+}(t_i)$ is unknown, we are looking for a solution with a particular $B_{H^+}^*$ for this equation system, whose roots also satisfy Eq. (47), giving back $B_{H^+}^*$. For this purpose, we used the uniroot function of programming language R (version 3.1.2; 31 October 2014), which is able to find this $B_{H^+}^*$. $B_{H^+}^*$ provides the $H^+$ budget in the given time step and finally, pH can be calculated as pH $= -\log_{10}(B_{H^+}^*/B_{H_2O})$.

## 3 Measurement data used in the test simulation

The GAG model described in the preceding sections was developed to simulate $NH_3$ emission from a single urine patch. However, for testing the model we chose a field experiment where the $NH_3$ emission flux was measured from several urine patches deposited relatively close in time. The only experiment we are aware of with these features was conducted

by Laubach et al. (2012), who measured the $NH_3$ fluxes over a field covered with a regular pattern of urine patches.

In the experiment, 156 artificial urine patches were deposited within 45 min (see an overview of urine patch characteristics in Table 2) over a circular plot at an experimental site, in Lincoln New Zealand. In the middle of the plot $NH_3$ concentration was measured at five heights with Leuning samplers (Leuning et al., 1985) from which the fluxes were derived by different methods. For this study we used the fluxes calculated by Laubach et al. according to the mass balance (MB) method.

Soil samples were taken from 24 patches on the edge of the plot to measure soil pH, volumetric water content and mineral N content. Soil temperature was measured at two heights, and meteorological measurements were also carried out (from which we used wind speed, temperature, photosynthetically active radiation (PAR), sensible heat flux and atmospheric pressure data). For more details on measurements and flux calculation, see Laubach et al. (2012).

In addition to the available measurements, we also needed meteorological data that were not measured in the experiment: global radiation ($R_{glob}$) and RH. We obtained these data from the National Climate Database for New Zealand (NIWA, 2015).

We compared our model results with measurements of $F_t$, soil pH, and $\theta$ for the measurement period between 24 February 11:30 and 1 March 2010 01:30 a.m. UTC +13 hours. In the case of $F_t$, the length of the collecting period of each measurement varied mostly between 1–1.5 h for daytime measurements, and 7–7.5 h for the night-time measurements. As the time step of our model is 1 h and emission fluxes were not expected to change considerably over the night, we assumed that the measured average $NH_3$ flux over the collecting period is representative for the midpoint of the period, and we compared these to our model values in the time step closest to the midpoint of the corresponding measurements.

In addition, assuming that the change of the soil's mineral reduced nitrogen content ($NH_x$-N) is parallel with the $B_{TAN}$ in the model soil pore, we also compared these two parameters. All of the input data, as well as the measurement data we used to compare our model results, together with their modification for our hourly model run, are listed in Table 3.

To compare the measured and modelled $F_t$ for a single urine patch, we assumed that the great majority of $NH_3$ in the experiment of Laubach et al. (2012) was emitted from the urine patches. Therefore, we multiplied the observed fluxes by the effective source area (804.9 m$^2$ as calculated by Laubach et al., 2012), then divided it by the total area of the deposited 156 patches (Eq. 55; where $F_t^{single}$ stands for the converted measured flux).

$$F_t^{single} = \frac{F_t \times 804.9}{156 \times A_{patch}} \qquad (55)$$

To compare $\theta$ with the observations, we had to consider that the $\theta$ measurements were taken by using a sharp-edged metal ring that was pushed to about 5 mm to the soil. As the model simulates the water content of a 4 mm thick layer, the same water loss via evaporation would not result in the same volumetric water content as was measured in the 5 mm depth sample. Since none of the other soil modules have an effect on the water budget, we ran the model also with a $\Delta z$ of 5 mm to get results that are comparable with the measurements.

## 4 Test simulation

The results of the test simulation are summarized in Fig. 4 and Table 4. GAG captures the emission relatively well. Considering that compared to the complexity of the phenomena, we use a simple model, the Person's correlation coefficient (hereafter referred to as "correlation") for $NH_3$ flux, can be considered as relatively high ($r = 0.54$, $p = 0.01$). The model slightly overestimates the fluxes before the rain event on the second day and it rather underestimates the measured values after it. The total emissions over the whole period from a single patch (modelled: 1.78 g N, measured: 3.88 g N) was underestimated. However, the model is still capable of reproducing the daily pattern of emissions with the mid-day peaks (except on the second day).

Soil pH is well simulated before the rain event, but similarly to the emission fluxes, it is underestimated afterwards. Overall there was a high and significant correlation ($r = 0.75$), between the model and the measurements. The sudden pH drop at the beginning of the rain event is thought to be caused by the lack of handling of $CO_2$ emission in the basic version of the model (see Sect. 5.3 for further examination of this effect).

Despite the large error bars on the measured mineral reduced soil N, its tendency is fairly similar to that of the TAN budget simulated by GAG. This is supported also by the significant correlation ($r = 0.63$) between the two variables. The model performance in terms of volumetric water content is very good with a slight underestimation from the fourth day after urine application. The statistical analysis showed a high correlation of 0.92 at a 0.001 significance level.

Analysing the $NH_3$ emission, pH and TAN budget together, it can be concluded that the rain event affected all three variables considerably. As it can be seen in the measured $NH_x$-N and pH data set (Fig. 4), their values right after the rain event peaked close to the level (or even higher) of the first peaks, which were generated by urea hydrolysis. This suggests that urea breakdown might restart after the rain event, explaining the difference between the modelled and measured values.

The GAG model used here does not account for any retention of urine by vegetation; however, it is possible that this occurs in reality. For example, Doak (1952) found that the urine held on the leaf surfaces was 36 % of fresh herbage

**Table 3.** Measured data used as input and the base of comparison with the model results, together with their original time resolution and their conversion to hourly time resolution.

| Variable | Original time resolution | Adaptation to hourly time resolution |
|---|---|---|
| **Input data** | | |
| $\chi_a$ ($\mu$g N m$^{-3}$) | Various (2–10 hourly) | Interpolated for the required hours. |
| $u$ (m s$^{-1}$) – at 2.1 m <br> PAR ($\mu$mol m$^{-2}$ s$^{-1}$) <br> $T_{soil}$ ($^\circ$C) – at 2 cm <br> $p$ (kPa) <br> $H$ (MJ m$^{-2}$ h$^{-1}$) | Half hourly | Averaged for the given hour. |
| $P$ (mm) | Half hourly | Summed up for the given hour. |
| $T$ ($^\circ$C) – at 3.85 m | Half hourly | Averaged for the given hour then calculated to 2 m height considering the average temperature gradient 6.5 $^\circ$C km$^{-1}$: <br> $T$ (2 m) $=T$ (3.85 m)–0.0065 $\times$ 1.85 |
| $R_{glob}$ (MJ m$^{-2}$ h$^{-1}$)* <br> RH (%)* | Hourly | – |
| **Data used in the comparison** | | |
| $F_t$ ($\mu$g N m$^{-2}$ s$^{-1}$) | Various (2–10 hourly) | Measurements in the midpoints of the collection periods were considered as representative hourly averages. |
| $\theta$ (m$^3$ m$^{-3}$) <br> pH <br> NH$_x$-N ($\mu$g N (g soil)$^{-1}$) | Various (2–19 hourly) | Measurements in the given hour were considered as representative hourly averages. |

* From the National Climate Database for New Zealand (NIWA, 2015), all the other parameters were measured at the site.

**Table 4.** Statistics calculated for the comparison of the modelled and measured variables: root mean square error (RMSE), Pearson's correlation coefficient ($r$), the equation of the fitted least-squares equation ($x$ – observation, $y$ – model) and the level of significance of the correlation.

| Variable* | RMSE | Equation | $r$ | Level of significance |
|---|---|---|---|---|
| Ammonia emission flux | 43.06 $\mu$g N m$^{-2}$ g$^{-1}$ | $y = 34.63+0.50x$ | 0.54 | 0.01 |
| Soil pH | 0.56 | $y = 3.04+0.64x$ | 0.75 | 0.001 |
| Model TAN budget vs. measured soil NH$_x$-N | – | – | 0.63 | 0.01 |
| Volumetric water content | 0.05 m$^3$ m$^{-3}$ | $y = 0.10+0.67x$ | 0.92 | 0.001 |

* All the modelled and measured variables are the same as shown in Fig. 4. In the case of the emission flux, we compared the measured flux in the given measurement period with the value simulated at the time of the midpoint of the corresponding measurement period as explained in Table 2.

weight. In addition, the model assumptions do not allow the model soil pore to dry out (the minimum water content is at the permanent wilting point). In reality, however, the moisture content of urine retained on the leaf surfaces can evaporate easily and also some soil pores can completely dry out leaving behind the urine components undissolved. In such dry conditions, in lack of water urea hydrolysis stops. Then, after a rainfall, urea gets dissolved (as well as from the leaf surface it is washed into the soil) and hydrolysis can begin again, leading to a high peak in pH, TAN budget and con-

sequently, NH$_3$ emission (see the further model results presented in Sect. S4).

## 5 Sensitivity analysis for non-meteorological parameters

In the following subsections we investigated module by module (2LCCPM, TAN budget, soil pH and water budget), how the model responds if we change the most critical model fea-
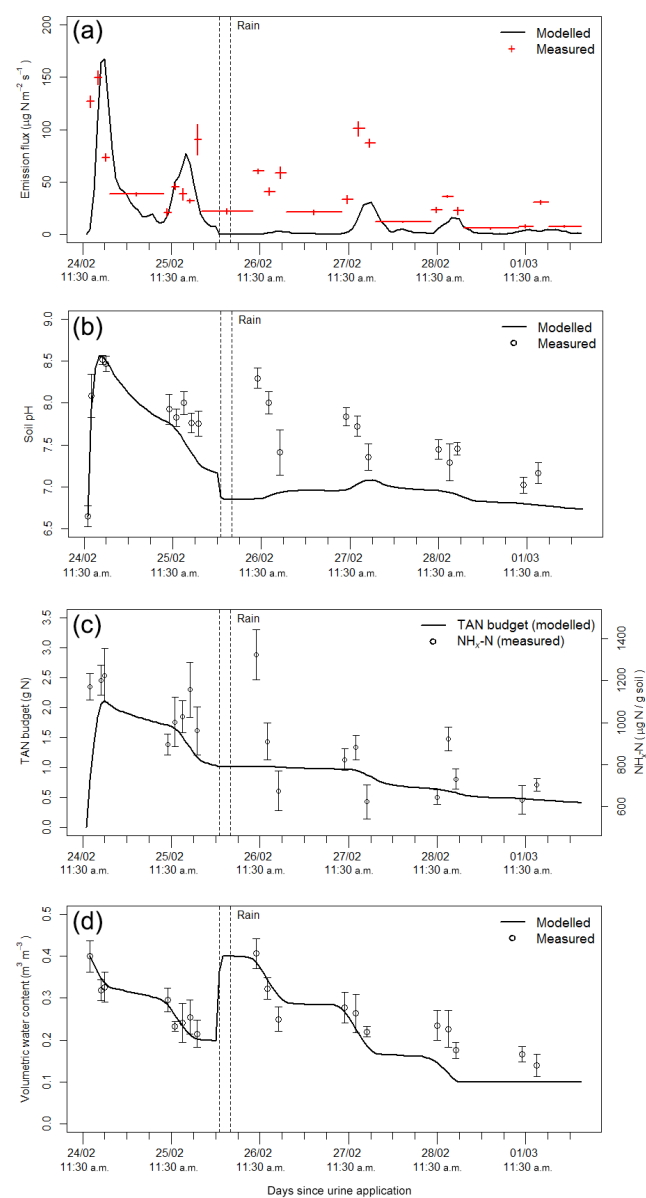
Figure 4. Comparison of modelled and measured values for $NH_3$ emission flux with the corresponding sampling periods of the measurements (a), soil pH (b), TAN budget and $NH_x$-N (c), and volumetric water content of the top 5 mm layer of the soil (d). The vertical error bars stand for the standard deviation in the measurements.

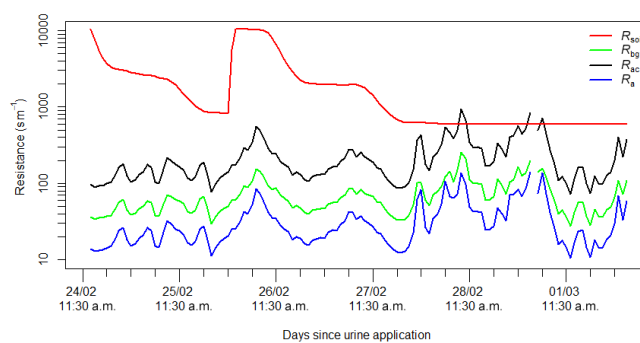tures. In the case of the model constants, we tested how the modelled total emitted $NH_3$ (1.78 g N from a urine patch) changes over the modelling period by increasing and decreasing the given assumed model constant by 10 and 20 %. An overview of the results can be seen in Table 5. Comments on this table are provided in the following subsections.



Figure 5. The atmospheric and the soil resistances over the modelling period. At the time of the missing values in $R_{bg}$, $R_{ac}$ and $R_a$ $u_*$ was 0, for which resistances are infinite. In these cases emission flux was assumed to be 0.

## 5.1 Sensitivity to atmospheric resistances

As the net $NH_3$ flux is dominated by the soil emission flux (shown in Fig. S1 in the Supplement) we investigated here only the influence of the atmospheric resistances that affect the soil emission: $R_{soil}$, $R_{bg}$, $R_{ac}$ and $R_a$. In Fig. 5, on the logarithmic scale it can be clearly seen that $R_{ac}$ is the only atmospheric resistance that reaches the magnitude of the estimated $R_{soil}$.

For the simulation the main driver in temporal variation in $R_{soil}$ is the actual volumetric water content (see Fig. 4). In the case of $R_a$, $R_b$, and $R_{bg}$ there is at least one order of magnitude difference compared to the soil resistance, illustrating how the model performance is much less sensitive to the exact values of $R_a$, $R_{ac}$, and $R_{bg}$. The close temporal correlation of all these atmospheric resistances illustrates how they are all controlled by variations in wind speed and stability for a single canopy type. All the atmospheric resistances are the closest to the soil resistance when weak wind (large atmospheric resistances) is coupled to dry soil conditions (small soil resistance).

Among $R_{bg}$, $R_{ac}$ and $R_a$, the parametrization of $R_{bg}$ is the most uncertain. As Table 5 shows, the model is hardly sensitive to the value of $z_1$. In addition, $u_{*g}$, as formulated by Nemitz et al. (2001; Eq. S15), can also change in wide ranges without significantly affecting soil emission: $R_{bg}$ could overcome the effect of $R_{soil}$ on $NH_3$ emission only with a 10 times higher value of $u_{*g}$.

## 5.2 Sensitivity to the estimation of the TAN budget

The two uncertain factors in the estimation of the TAN budget are the thickness of the source layer ($\Delta z$) and the area of the patch ($A_{patch}$). Originally the model was run with a $\Delta z$ of 4 mm; however, the sensitivity analysis showed (Table 5) that the change in total emission is approximately half of the change in $\Delta z$. Therefore, this source of error must be considered when model results are evaluated.

**Table 5.** The percentage of the change in total emitted $NH_3$ compared to the original run after modifying the different model constants by $-20$, $-10$, $+10$ and $+20\%$.

| Module | Parameters | Total $NH_3$ emission change in response to change if parameter by | | | |
|---|---|---|---|---|---|
| | | $-20\%$ | $-10\%$ | $+10\%$ | $+20\%$ |
| 2LCCPM | $z_l$ (height of the top of logarithmic wind profile) | $+0.02\%$ | $+0.01\%$ | $-0.01\%$ | $-0.02\%$ |
| TAN budget | $\Delta z$ (thickness of $NH_3$ emission layer) | $-11.7\%$ | $-5.57\%$ | $+5.07\%$ | $+10.5\%$ |
| | $A_{patch}$ (area of a urine patch) | $+1.39\%$ | $+0.67\%$ | $-0.58\%$ | $-1.61\%$ |
| Soil pH | $\beta$ (soil buffering capacity) | $+1.29\%$ | $+0.64\%$ | $-0.62\%$ | $-1.22\%$ |
| Water budget | REW (readily evaporable water) | $-2.98\%$ | $-1.69\%$ | $+2.06\%$ | $+4.32\%$ |
| | $\theta_{fc}$ (field capacity) | $-18.4\%$ | $-6.63\%$ | $+6.34\%$ | $+9.12\%$ |
| | $\theta_{pwp}$ (permanent wilting point) | $+9.48\%$ | $+4.60\%$ | $-4.42\%$ | $-8.85\%$ |

We also tested the model with $\Delta z$ values between the ranges reported by Laubach et al. (2012; Fig. 6), and we found that the smaller the value of $\Delta z$, the higher the emission peak after urine application and the smaller the emission peaks in the following days. Firstly, this is caused by a smaller value of $R_{soil}$, due to the thinner source layer. Secondly, since the thinner layer can store less TAN in total, the source layer runs out of TAN more quickly leading to lower peaks in the later part of the modelling period.

In addition, we carried out a simulation with the maximum value of $\Delta z$, the penetration depth of incoming urine. Considering a soil layer with a thickness of $y$ (dm), its water content can be expressed as $A_{patch} \times y \times (\theta_{fc} - \theta_{pwp})$. In this way, the urine deposited in a single patch ($W_{urine}$) in this experiment will fill up a $y = 0.2\,dm = 20\,mm$ thick soil layer. In this case, $R_{soil}$ is at least 5 times higher than in the original run (or even bigger as there is more water in the source layer and, consequently, the layer dries out more slowly), that prevents $NH_3$ from escaping from the soil shortly after urine deposition. However, from the second day due to the higher available TAN budget, the fluxes are closer to the measurements.

In contrast to $\Delta z$, the model does not appear to be very sensitive to $A_{patch}$, with even a $+20\%$ change causing less than 2% change in total emission (Table 5). Laubach et al. (2012) estimated that the patches gradually grew by lateral diffusion, so that the area of the patches had doubled over the modelling period at the measurement site. Therefore, we conducted a simulation with GAG with a gradually growing patch, whose area doubles by the end of the period. In Fig. 7 we show the measured emission fluxes in relation to constant and gradually increasing values of $A_{patch}$, with the model results expressed for the whole area (converted based on the reorganized form of Eq. 55).

The largest difference with the growing patches, compared with the original run, occurred over the first 2 days. Then,

the emission rates became smaller for the growing patches than with the constant patch area. The difference is a consequence of the combined effect of the growing source area ($156 \times A_{patch}(t_i)$) and the changing emission flux from a single patch.

In our model if a urine patch grows, it means physically that the initial liquid content is diffusing in the soil horizontally, leading to gradually declining volumetric water content. In addition, the evaporating area grows simultaneously, further intensifying the decrease of water content. Thus, $R_{soil}$ will be smaller, allowing stronger $NH_3$ emissions in the first 2 days. This leads to lower TAN budget in the second half of the period, resulting in slightly smaller emissions than in the original run.

Finally, it has to be pointed out that we neglect an effect where the presence of hippuric acid in urine may increase urea hydrolysis and consequently, $NH_3$ emission (Whitehead et al., 1989). Whitehead et al. found that ignoring this triggering effect can lead to up to $-10\%$ difference in the cumulative $NH_3$ volatilization (expressed as the proportion of the total nitrogen content of urine) compared to real urine containing the same amount of urinary N.

In the measurement campaign (Laubach et al., 2012) an artificial urine solution was spread on the experimental plot that was enriched with additional urea, so we compared a urea based model with a concentrated urea solution. Therefore, the difference in modelled and measured $NH_3$ fluxes, originating from this simplification, is possibly negligible, though it could be relevant if the model is applied in a real grazing situation. However, Whitehead et al. (1989) reported comparable differences in $NH_3$ emissions when they compared urea+hippuric acid solutions with different total N contents as well as different hippuric acid ratios.

The N content of urine ranges widely, not just amongst different animals, but also for different urination events by the same animal (Betteridge et al., 1986; Hoogendoorn et
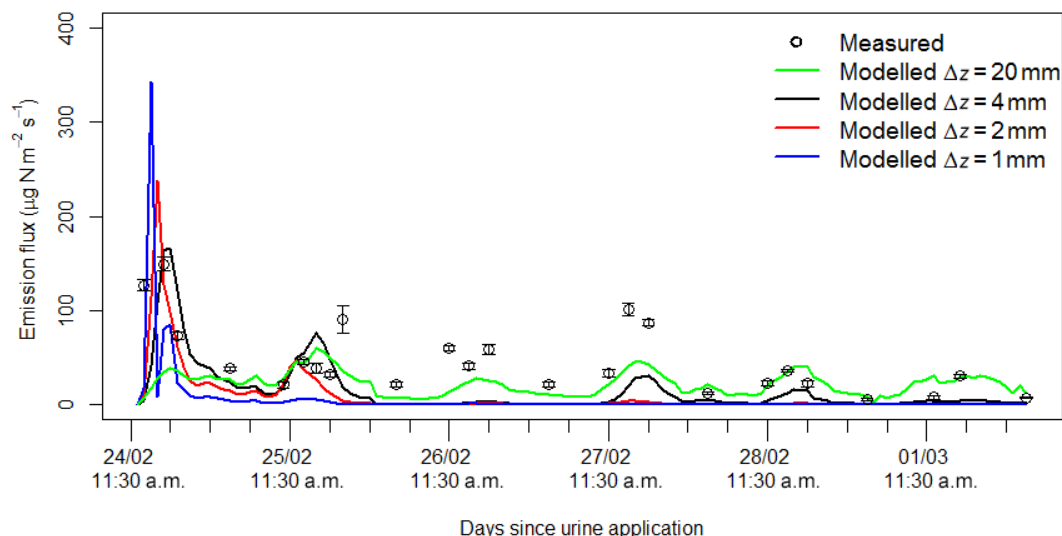
**Figure 6.** $NH_3$ fluxes from a urine patch with different $\Delta z$ values.
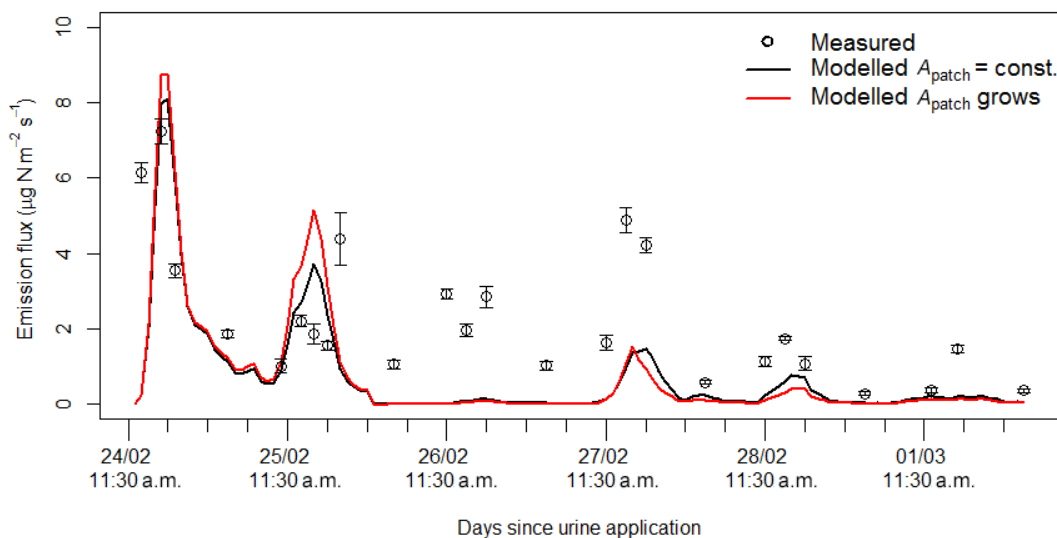


**Figure 7.** $NH_3$ fluxes from the whole experimental area with constant and with gradually growing urine patches.

al., 2010). This means that assuming an average N concentration of 8 g, according to Whitehead et al. (1989) can result in a 10 % overestimation in the cumulative volatilization of ammonia if the real nitrogen concentration was as low as $2\,g\,L^{-1}$. Similarly, in the case of the different ratios of hippuric acid and urea: if we assume that the hippuric acid N is an average of 0.8 % of the urea N (based on the data published by Dijkstra et al. (2013) this proportion varies between 1.4–0.36 %), according to Whitehead et al. (1989), the overestimation of the cumulative ammonia emission can be 10 % if the proportion of hippuric acid was minimal in reality.

As the effect of hippuric acid on urea hydrolysis is not widely investigated in the literature, at the moment the current approach is the best we can achieve to simulate the

decomposition chemistry in urine. Although the field scale model would most likely underestimate ammonia emission due to the exclusion of the effect influence of hippuric acid, this underestimation may be partly balanced by the sources of overestimation in the model. Nonetheless, this uncertainty should be addressed when the model is applied on field scale.

## 5.3 Uncertainties in the estimation of soil pH

The main uncertainty in the model pH calculation is the applied buffering capacity ($\beta$). Apparently, the model is not highly sensitive to the tested changes of $\beta$; however, using the same $\beta$ for every soil type could lead to errors in $NH_3$ emission estimation. Therefore, we tested the model with two
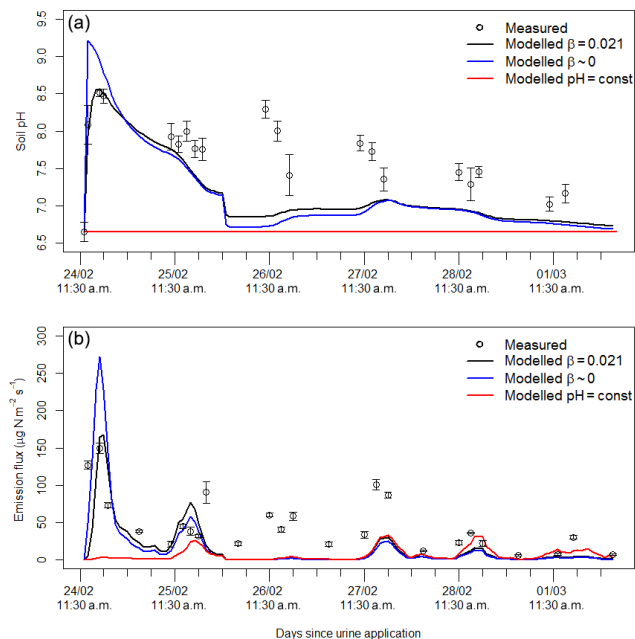
**Figure 8.** Soil pH under a urine patch **(a)** and $NH_3$ emission from it **(b)** with the currently applied buffering capacity ($\beta = 0.021$, original run), with no buffering ($\beta = 0$) and with constant pH, together with the measured values.



**Figure 9.** Soil pH under a urine patch **(a)** and $NH_3$ emission from it **(b)** without $CO_2$ emission (original run) and with an assumed $CO_2$ emission. On panel **(a)** the original run without rain is also plotted.

contrasting assumptions about buffering capacity: (a) when the system is totally buffered (pH is constant) and (b) when there is no buffering effect ($\beta = 0$). For the constant pH scenario, we chose the soil pH measured before the deposition of the urine patches (pH = 6.65).

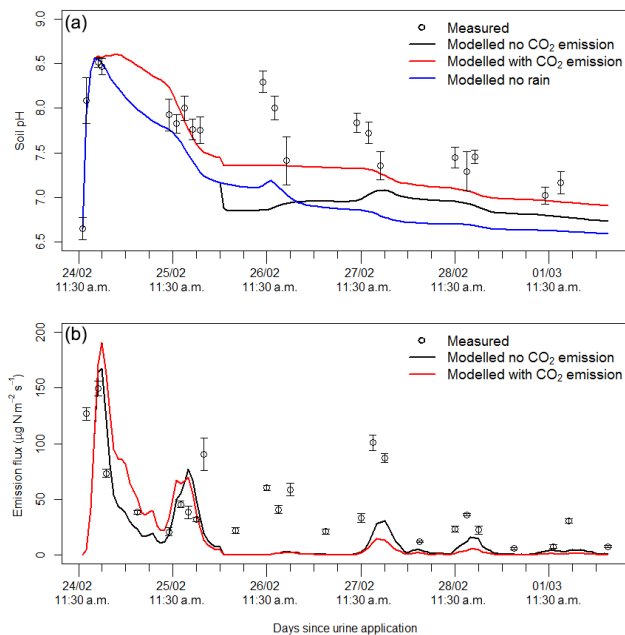The results show (Fig. 8) that with a constant soil pH, GAG fails to capture the first, dominant peak in emission. This suggests that dynamic modelling of pH is necessary for a proper estimation of $NH_3$ emission. By contrast, with $\beta = 0$ the model overestimates the first emission peak, while there is little difference in $NH_3$ fluxes in the rest of the period. Thus, with $\beta = 0$ the model is still capable of reproducing the daily cycle of $NH_3$ emission.

Another feature of the model which affects the pH as well as the emission flux calculation is the handling of $CO_2$ emission following urine deposition (as discussed in Sect. 2.6). A sudden drop can be seen in the simulated pH at the beginning of the rain event (Fig. 4b), which tends to disappear if there is no rainfall over the modelling period (Fig. 9a, blue line).

At the beginning of the rainfall the volume of the gaseous part of the model soil pore suddenly shrinks as the liquid part grows with the incoming water. As a result (given that the base model does not allow $CO_2$ emission), gaseous $CO_2$ accumulates in the soil pore and is forced to dissolve into the liquid phase. This intensifies the formation of carbonic acid and its subsequent dissociation, leading to a significant drop in pH.

In the experiment by Wang et al. (2013) $CO_2$ emission over urine patches peaked within 8 h after urine application, while both Ma et al. (2006) and Lin et al. (2009) found that the first peak of $CO_2$ emission occurred on the first day. In addition, Lin et al. (2009) reported a high correlation ($r = 0.63$) between $CO_2$ emission and soil temperature, suggesting a strong temperature dependency (similarly, we found a correlation of 0.58 for $NH_3$, see Table 6).

Based on the above similarities between the temporal development of $NH_3$ and $CO_2$ emission, to test the effect of $CO_2$ emission on the GAG simulations, we assumed that the amount of emitted $CO_2$ is half of the emitted $NH_3$ in moles (similarly to urea hydrolysis where from one urea molecule two $NH_4^+$ and one $HCO_3^-$ ions are produced). Even if this is a simplification for $CO_2$ emission, the results show the potential of future more comprehensive incorporation of the process into the model. By accounting for $CO_2$ emission the modelled pH values were found to be closer to the measured ones, while the sudden drop at the start of the rain event also largely disappeared (Fig. 9). As a consequence of these changes, the $NH_3$ emission fluxes were larger before the second day and – due to the larger loss in TAN budget – were smaller in the latter part of the experiment.

The apparently contradictory results with the assumed $CO_2$ emission above – better agreement in pH and poorer agreement in the $NH_3$ fluxes – suggest that the TAN in the model soil pore is depleted too early, leading to a significant underestimation of the emission fluxes in the second part of the modelling period. Two scenarios can be envisaged that

**Table 6.** The results of the sensitivity analysis to the different meteorological variables. We changed these by $\pm \Delta x$ derived based on the minimum and the maximum of the given parameter over the modelling period ($\Delta x = (\text{Max–Min})/10$), and calculated the difference in the total emission over the modelling period compared to the original run. We also calculated the correlation ($r$) between the original input variables and the modelled hourly $NH_3$ emission fluxes.

| Variable | Min | Max | $\Delta x$ | Total $NH_3$ emission change in response to change in parameter by | | |
| --- | --- | --- | --- | --- | --- | --- |
| | | | | $-\Delta x$ | $+\Delta x$ | $r$ |
| $u$ (ms$^{-1}$) | 0.62 | 8.59 | 0.80 | $-5.5\%$ | $+4.7\%$ | 0.40 |
| $T_{soil}$ (°C) | 11.6 | 27.9 | 1.64 | $-2.6\%$ | $+2.7\%$ | 0.58 |
| $p$ (kPa) | 99.9 | 102.3 | 0.24 | $+0.0\%$ | $-0.0\%$ | $-0.33$ |
| $T_{air}$ (°C) | 13.5 | 29.0 | 1.56 | $-2.4\%$ | $2.9\%$ | 0.60 |
| $R_{glob}$ (MJ m$^2$ h$^{-1}$)[a] | 0.00 | 3.32 | 0.33 | $-2.0\%$ | $+4.1\%$ | 0.32 |
| RH (%)[b] | 30 | 95 | 6.50 | $+9.1\%$ | $-8.6\%$ | $-0.49$ |
| RH (%)[b] | only for evaporation[c] | | | $+3.2\%$ | $-2.8\%$ | – |
| $P$ (mm)[d] | 0.00 | 0.83 | 0.08 | $-0.7\%$ | $+0.8\%$ | – |
| $T_{air}$ and $T_{soil}$ (°C) | – | – | – | $-4.9\%$ | $+5.7\%$ | – |

[a] When changed by $-\Delta x$, negative values were replaced by 0. [b] When changed by $+\Delta x$, values greater than 100 % were reduced to 100 %. [c] In this test RH was modified by the same extent but only in the evaporation module. [d] The hourly precipitation sum was changed only in the hours when there was precipitation originally.

could cause this effect: scenario (1) the simulated rate of urea hydrolysis is higher than it is in reality, or scenario (2) at the experimental site fresh urea that had been intercepted by leaves and dried onto leaf surfaces, was washed to the soil during the rain event, thereby maintaining $NH_3$ emission afterwards.

As we discussed in Sect. 4, the measurement data also suggest the feasibility of scenario (2). Therefore, we tested the model – assuming that 10 % of the applied urine was intercepted on the leaf surface – with 1.5 g of urea washed in during the rain event (see Sect. S4). With this assumption the modelled values were in better agreement with observations not only in the case of $NH_3$ exchange flux (Fig. 10d) but also the TAN budget and soil pH (see both at Fig. S2). These results clearly support the idea of the possible restart of breakdown of the fresh urea penetrating to the soil dissolved in rain water.

## 5.4 Uncertainties in the estimation of the water budget

The GAG model is found to be sensitive to model constants related to the water budget, especially field capacity, $\theta_{fc}$ (Table 5). The high sensitivity to a low value of $\theta_{fc}$ appears to be because this limits the amount of urine which remains available for hydrolysis and $NH_3$ emission from the source layer. In addition, we also found large differences in total ammonia emission when we modified the permanent wilting point. On regional scale it is not likely to have a database of measured $\theta_{fc}$ and $\theta_{pwp}$ values over a dense grid. It is more feasible that a soil texture map can be used for this purpose with recommended values of $\theta_{fc}$ and $\theta_{pwp}$ values for different soil types. Both $\theta_{fc}$ and $\theta_{pwp}$ can have an uncertainty of $\pm 20\%$ (e.g. in Allen et al., 1998 for sandy loam $\theta_{fc} = 0.18$–0.28), similarly

to the extent of modification in the current sensitivity test. Therefore, at regional application, this uncertainty has to be considered when interpreting the model results.

In addition, a limitation of the calculation of the water budget is that GAG does not account for the water movement in the soil, including the effect of capillary force, diffusion of water in the soil as well as the concentration of TAN and urea within the moving liquid. However, the simulation of these processes is very complex. Shorten and Pleasants (2007) published a system of partial differential equations describing these processes, which could be a basis for further development of GAG.

## 6 Sensitivity to meteorological factors

For quantitative comparison, we show a variety of meteorological factors and the hourly $NH_3$ emission fluxes in Fig. 10. The $NH_3$ emission flux peaks almost every day shortly after midday, when soil temperature reaches its maximum. The only exception is the second day after urine application when the curve of emission flux stayed flat in the simulation, which was linked to the rain event as discussed in the previous sections.

The close relationship between the soil as well as the air temperature and $NH_3$ emission fluxes can be also seen in the calculated high correlations ($r = 0.58$ and $r = 0.60$, respectively). Compared with the other meteorological factors (Table 6) the relationship with these two seems to be the strongest. Relative humidity apparently has a slightly weaker, but still considerable role in the simulated $NH_3$ volatilization ($r = -0.49$). Based on the correlation values, there was a weaker relationship with wind speed ($r = 0.40$), which may
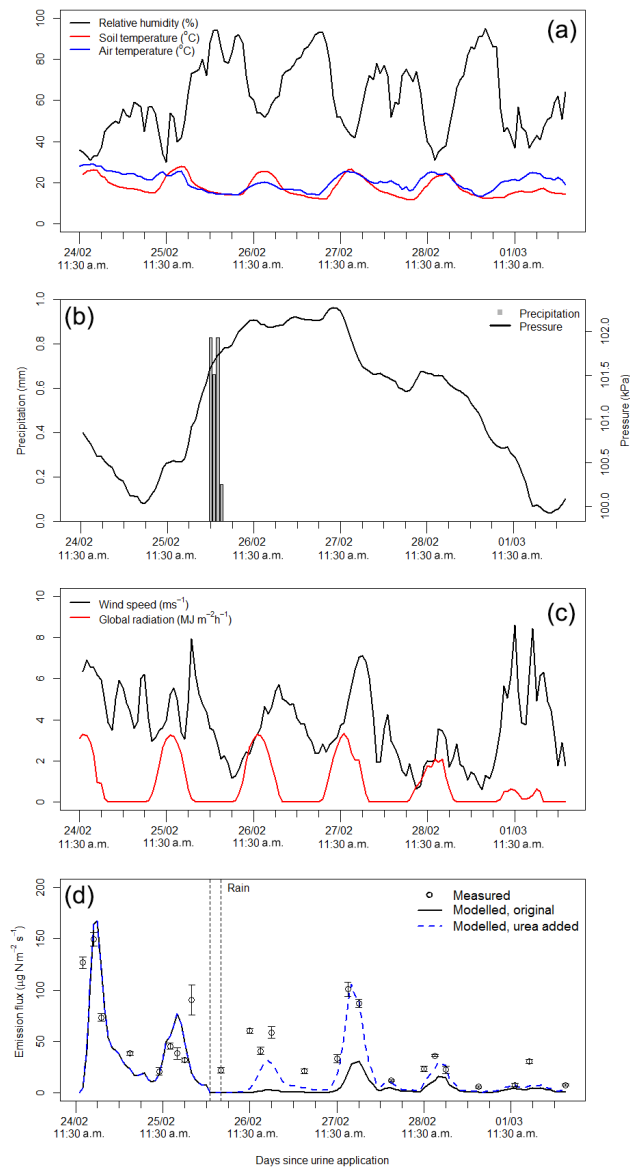
**Figure 10.** The investigated meteorological variables (relative humidity, soil, and air temperature **(a)**, precipitation and surface pressure **(b)**, wind speed and global radiation **c)** and the hourly $NH_3$ fluxes **(d)** simulated by the original model (black line) and the modified model (dashed blue line), in which fresh urea was assumed to be washed into the soil during the rain event.

be related to the fact that simulated $R_{soil}$ provided a much larger constraint on $NH_3$ soil emission than the atmospheric resistances (Fig. 5). Global radiation as well as atmospheric pressure indicated a weaker influence (lower than $r = 0.40$ in absolute value) on the simulated $NH_3$ emission.

We also carried out a sensitivity analysis to the different meteorological parameters. To test the sensitivity to a given parameter, we modified it, while keeping all the other parameters the same, and we ran a simulation with GAG. At the end of every simulation we calculated the total ammonia

emission over the period, and expressed it as the percentage difference compared to the total emission in the original run. To get comparable results, we modified the original data sets in every case by $\pm \Delta x$, calculated as 10 % of the difference between the measured minimum and maximum value of the given parameter over the modelling period.

Table 6 shows that $NH_3$ emission is the most sensitive to relative humidity (the differences in total emission were $+9.1$ and $-8.6$ %) and wind speed (the differences were $-5.5$ and $4.7$ %). In addition, a relatively high difference ($+4.1$ %) was observed in the case of global radiation when its values were raised by $\Delta x$.

In spite of the high correlations, when soil and air temperature were modified separately, we got relatively small anomalies in the total emissions (less than 3 % in absolute value for both soil and air temperature). However, when air and soil temperature were adjusted together (assuming that the change of these two temperature parameters is parallel), the differences were larger (see Table 6). Only low sensitivity was detected in the case of atmospheric pressure and hourly precipitation.

The results for wind speed and the different temperature parameters can be easily explained. Wind plays a governing role in turbulent mixing of the quasi-laminar and turbulent layer; consequently, it has a considerable effects on the vertical atmospheric transfer of ammonia. Regarding temperature, urea hydrolysis as well as the compensation point both in the stomata and the soil pores follow an exponential function of temperature.

Sutton et al. (2013) used a metric, $Q_{10}$, to express the relative increase in $NH_3$ emission over a range of 10 °C. We derived $Q_{10}$ by running the model with 10 °C higher air and soil temperature. The resulted value of 1.26 compared to that reported by Sutton et al. for grazing (4.7 for sheep sites) suggest a rather modest temperature sensitivity. The model showed similarly modest sensitivity when we tested it with three and five times higher N concentration in urine (allowing more TAN in the later stages of the modelling period; Table 7). Based on this results it can be concluded that the lower $Q_{10}$ values are not a consequence of the limited TAN available in the later stages of the modelling period.

A possible explanation for the difference between the reported and the simulated temperature sensitivity can be the temporal development of $Q_{10}$ over time (Fig. 11). We calculated the $Q_{10}$ values for every time step as the ratio of the cumulative emissions from the higher temperature model version and the original one, and we found that $NH_3$ emission is more sensitive to temperature in the first 6 h than in the later stages. Considering that over a grazed field urine patches are deposited in every time step, creating a peak in the individual patch emissions, the total emission for the whole field will be presumably more sensitive to temperature than that for a single urine patch.

RH has a dual effect on $NH_3$ emission. Firstly, it plays a vital role in the water budget and secondly, it also influences

**Table 7.** Comparison of the total emission (g N) from a single urine patch from the model runs assuming different N content of the urine deposited with the original temperature and $+10\,^\circ\mathrm{C}$ (both in air and the soil temperature) scenario. We also calculated $Q_{10}$ as the ratio of the total emission for the original and the amended temperature scenario.

| | Total emission (g N) | | |
|---|---|---|---|
| | Original | $+10\,^\circ\mathrm{C}$ | $Q_{10}$ |
| Base run | 95.8 | 121.0 | 1.26 |
| $3 \times$ N content | 290.4 | 370.8 | 1.28 |
| $5 \times$ N content | 489.7 | 613.8 | 1.25 |
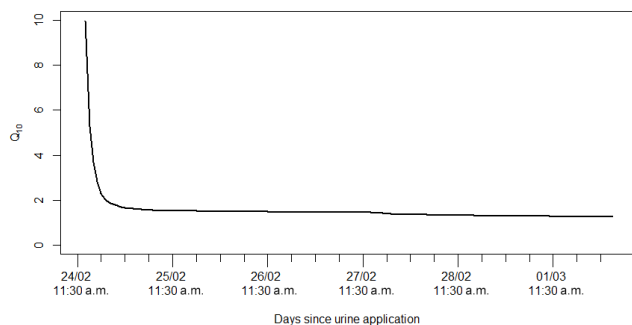


**Figure 11.** Calculated $Q_{10}$ values for the cumulative $NH_3$ emissions between urine application and the given time step.

the deposition of ammonia to the leaf surface. We tested the sensitivity in a model scenario where relative humidity was modified only in evaporation, and we observed only a $+3.2\,\%$ difference for $-\Delta x$ and $-2.8\,\%$ for $+\Delta x$ change. This clearly suggests that the effect of RH on $NH_3$ emission in GAG is stronger through deposition to leaf surfaces than through soil evaporation.

The physical explanation for the opposite change in RH and the total emission is that at higher values of relative humidity the formation of a water film on the leaf surface is more likely. As a result, deposition is more effective (see the different fluxes in Fig. S1), which will generate a loss in the net emission flux over the whole system (including the exchange with soil and stomata as well as the deposition to cuticle).

Although precipitation was shown to suppress modelled emission, the total emission over the period was not strongly sensitive to a change of $\pm 10\,\%$ ($\pm 0.08$ mm; Table 6). This is a result of the model features that (1) allow only a $(\Delta z \times (\theta_{\mathrm{fc}} - \theta_{\mathrm{pwp}}) =) 1.2$ mm of maximum liquid content in the model soil pore and (2) do not allow wash out TAN from the source layer. Therefore, in the GAG model even a heavy rain event ($> 6$ mm h$^{-1}$) – apart from the slight effect on evaporation – has the same effect as a modest 1.2 mm h$^{-1}$ of precipitation. In the test simulation during the rain event the soil reached its maximum water content ($\theta_{\mathrm{fc}}$). We found

that by decreasing the amount of total precipitation so that the soil does not reach $\theta_{\mathrm{fc}}$, the maximum difference in total emission was $+3\,\%$.

In addition, the timing of the rain event can also lead to a difference in total $NH_3$ emission due to the associated increase in $R_{\mathrm{soil}}$ which tends to suppress the rate of volatilization. We found that the timing of the rain event affects the $NH_3$ emission, with up to a $6\,\%$ reduction or $2\,\%$ increase in the total $NH_3$ emission (see the model results in Sect. S5). Nevertheless, it must be emphasized that in reality $NH_3$ can escape from wet soil not only through gaseous diffusion in the empty soil pores. Dissolved $NH_3$ may get to the soil surface also through the solution and can be volatilized from there (Cooter et al., 2010). This is not taken into account in the present soil resistance parametrization. Therefore, the effect of rainfall might not be as strong as this experiment showed. On the other hand, as we mentioned earlier, during a dry period urea hydrolysis may slow or stop in the absence of water. If the rainfall begins after such a dry period, by restarting urea hydrolysis, it can even enhance ammonia emission rather than suppress it.

## 7 Discussion

We constructed a novel $NH_3$ emission model for a urine patch (GAG) that is capable of simulating the TAN and the water content of the soil under a urine patch and also soil pH (see the list of all the model parameters and variables together with their abbreviations in Table 8). The difference between the simulated and measured values suggested that to improve the model, further investigation is needed regarding the effect of a possible restart of urea hydrolysis with rain events also soil pH.

The sensitivity analysis to the uncertain parameters showed that soil resistance had more than an order of magnitude stronger effect on soil $NH_3$ emission than the atmospheric resistances. An exceptional case is when weak wind is coupled with dry soil, in which case atmospheric and soil resistances may become comparable.

Our sensitivity analysis also showed that if the thickness of the source layer ($\Delta z$) is modified by a given percentage, the difference in the resulting total ammonia emission over the modelling period will be half of this percentage. Therefore, this source of error must be considered when model results are evaluated. Future work should also consider how independent data sets can help characterize the depth of the effective soil emission layer, as well as consider how both downward and upward migration of TAN with deeper soil layers can be addressed.

In the case of pH we showed that process-based modelling of pH is necessary to reproduce the very first high peak in $NH_3$ emission. The simulations were carried out with an assumed soil buffering capacity. While this affects the timing of emissions, we found that the total emission is not sensitive

**Table 8.** Abbreviations.

| Abbreviation (unit) | Model variable |
|---|---|
| $\frac{D_{O_3}}{D_{NH_3}}$ | Ratio of diffusivity of $O_3$ and $NH_3$ |
| $[X]$ (mol dm$^{-3}$) | Concentration of compound $X$ |
| $A$ | Parameter for calculating $R_w$ |
| $A_h$ | Parameter for urea hydrolysis simulation |
| $A_{patch}$ (m$^2$) | Area of a urine patch |
| $B_C$ (mol) | Carbon content of the source layer (originating from urea) |
| $B_{H_2O}$ (dm$^3$) | Water budget in the source layer |
| $B_{H_2O}(max)$ (dm$^3$) | Maximal water amount in the source layer |
| $B_{H_2O}(min)$ (dm$^3$) | Minimal water amount in the source layer |
| $B_{H_2O}'$ (dm$^3$) | Precalculated water budget in the source layer |
| $B_{H_2O}^{Tot}$ (dm$^3$) | Total water budget under a urine patch |
| $B_N$ (mol) | TAN + gaseous ammonia content in the source layer |
| $B_{TAN}$ (g N) | TAN budget in the source layer |
| $B_{urea}$ (g N) | Urea budget under a urine patch |
| $B_X$ (mol) $(X = H_2CO_3, HCO_3^-, CO_3^{2-},$ $CO_{2(g)}, NH_4^+, NH_{3(aq)}, NH_{3(g)}, H^+)$ | Budget of a chemical compound $X$ under the urine patch |
| $C_d$ | Effect of day and night on evapotranspiration |
| $c_N$ (N dm$^{-3}$) | N content of the urine |
| $c_N^{Tot}$ (g N dm$^{-3}$) | Urine N content after dilution in the soil |
| $D_g$ (m$^2$ s$^{-1}$) | Diffusivity of $NH_3$ in air |
| $E$ (mm h$^{-1}$) | Soil evaporation rate |
| $e_a$ (kPa) | Actual water vapour pressure |
| $e_s$ (kPa) | Saturated water vapour pressure |
| ET (mm h$^{-1}$) | Actual evapotranspiration rate |
| ET$_0$ (mm h$^{-1}$) | Reference evapotranspiration rate |
| $f_c$ (m$^2$ m$^{-2}$) | Vegetation coverage |
| $F_f$ ($\mu$g N m$^{-2}$ s$^{-1}$) | $NH_3$ exchange flux with the foliage |
| $F_g$ ($\mu$g N m$^{-2}$ s$^{-1}$) | $NH_3$ exchange flux over the ground |
| $F_{sto}$ ($\mu$g N m$^{-2}$ s$^{-1}$) | $NH_3$ exchange flux with stomata |
| $F_t$ ($\mu$g N m$^{-2}$ s$^{-1}$) | Total $NH_3$ exchange flux over the canopy |
| $f_w$ (m$^2$ m$^{-2}$) | Wetted uncovered soil fraction |
| $F_w$ ($\mu$g N m$^{-2}$ s$^{-1}$) | $NH_3$ deposition flux to water and waxes on the leaf surface |
| $G$ (MJ m$^2$ h$^{-1}$) | Soil heat fux |
| $g_{light}$ | Relative conductance for the effect of light on $g_s$ |
| $g_{max}$ (mmol $O_3$ m$^{-2}$) | Maximal stomatal conductance |
| $g_{min}$ | Minimal relative stomatal conductance |
| $g_{pot}$ | Relative stomatal conductance for the effect of plant phenological state on $g_s$ |
| $g_s$ (mmol $O_3$ m$^{-2}$) | Stomatal conductance for $O_3$ |
| $g_{SWP}$ | Relative conductance for the effect of soil water on $g_s$ |
| $g_{temp}$ | Relative conductance for the effect of temperature on $g_s$ |
| $g_{VPD}$ | Relative conductance for the effect of vapour pressure deficit on $g_s$ |
| $H(X)$ (mol dm$^{-3}$ (mol dm$^{-3}$)$^{-1}$) | Henry coefficient for the given gas $X$ |
| $i_C$ (mol) | Carbon input to the urine patch |
| $i_N$ (mol) | TAN input to the urine patch (TAN production in moles) |
| $K(X)$ (mol dm$^{-3}$) | Dissociation constant for the given compound $X$ |
| $K_c$ | Crop coefficient |
| $K_{cb}$ | Transpiration coefficient |
| $K_e$ | Soil evaporation coefficient |
| $k_h$ | Urea hydrolysis constant |
| $L$ (m) | Monin-Obukhov length |
| LAI (m$^2$ m$^{-2}$) | Leaf area index |
| $N_{app}$ (kg N ha$^{-1}$) | Nitrogen applied over a urine patch |
| $N_{prod}$ (g N) | TAN production |

**Table 8.** Continued.

| Abbreviation (unit) | Model variable |
|---|---|
| $P$ (mm) | Precipitation |
| PAR ($\mu$mol m$^2$ s$^{-1}$) | Photosynthetically active radiation |
| $Q_{10}$ | Relative increase in NH$_3$ emission over a range of 10 °C |
| $R_a$ (s m$^{-1}$) | Aerodynamic resistance over the canopy |
| $R_{ac}$ (s m$^{-1}$) | Aerodynamic resistance in the canopy |
| $R_b$ (s m$^{-1}$) | Resistance of the quasi-laminar layer over the canopy |
| $R_{bg}$ (s m$^{-1}$) | Resistance of the quasi-laminar layer in the canopy |
| REW (mm) | Readily evaporable water in the soil |
| $R_{glob}$ (MJ m$^2$ h$^{-1}$) | Global radiation/solar radiation |
| RH (%) | Relative humidity |
| $R_n$ (MJ m$^2$ h$^{-1}$) | Net radiation |
| $r_{RX}$ (mol) | Consumption or production of a given compound in reaction $X$. |
| $R_{soil}$ (s m$^{-1}$) | Soil resistance |
| $R_{sto}$ (s m$^{-1}$) | Stomatal resistance |
| $R_{sto}$ (O$_3$)(s m$^{-1}$) | Stomatal resistance for O$_3$ |
| $R_w$ (s m$^{-1}$) | Cuticular resistance |
| $R_w$ (min) (s m$^{-1}$) | Minimal cuticular resistance |
| $S_{MI}$ | Soil moisture index |
| $T$ (°C) | Air temperature at 2 m |
| $t_i$ | $i$th time step |
| $T_{soil}$ (°C) | Soil temperature |
| $u$ (m s$^{-1}$) | Wind speed |
| $u_*$ (m s$^{-1}$) | Friction velocity |
| $u_{*g}$ | Friction velocity at ground level in the canopy |
| $U_{add}$ (g N) | Urea added to the source layer |
| $V_{air}$ (dm$^3$) | Volume of the air in the source layer |
| $W_{evap}$ (dm$^3$) | Water loss as soil evaporation from the urine patch |
| $W_{rain}$ (dm$^3$) | Water input as rain water over the urine patch |
| $W_{urine}$ (dm$^3$) | Volume of urine |
| $z_1$ (m) | Height of the top of logarithmic wind profile |
| $z_w$ (m) | Height of wind measurement |
| $\alpha$ | Parameter for calculating $R_{ac}$ |
| $\beta$ (mol H$^+$ (pH unit)$^{-1}$ dm$^{-3}$) | Soil buffering capacity |
| $\beta_{patch}$ (mol H$^+$ (pH unit)$^{-1}$) | Buffering capacity of the source layer |
| $\gamma$ (kPa °C$^{-1}$) | Psychometric constant |
| $\Gamma_p$ | NH$_3$ emission potential in the soil pore |
| $\Gamma_{sto}$ | NH$_3$ emission potential from the stomata |
| $\Gamma_{sto}$(max) | Maximal NH$_3$ emission potential from the stomata |
| $\Delta$ (kPa °C$^{-1}$) | Slope of saturation vapour pressure curve |
| $\Delta z$ (mm) | Thickness of the source layer |
| $\Delta z_E$ (m) | Thickness of the evaporation layer |
| $\theta$ (m$^3$ m$^{-3}$) | Volumetric water content |
| $\theta_{fc}$ (m$^3$ m$^{-3}$) | Field capacity |
| $\theta_{por}$ (m$^3$ m$^{-3}$) | Porosity |
| $\theta_{pwp}$ (m$^3$ m$^{-3}$) | Permanent wilting point |
| $\xi$ | Soil tortuosity |
| $\tau$ (days) | Decay parameter |
| $\chi_a$ ($\mu$g N m$^{-3}$) | Air concentration of NH$_3$ |
| $\chi_c$ ($\mu$g N m$^{-3}$) | Compensation point above the vegetation |
| $\chi_p$ ($\mu$g N m$^{-3}$) | Compensation point in the soil pores |
| $\chi_{sto}$ ($\mu$g N m$^{-3}$) | Stomatal compensation point |
| $\chi_{z0}$ ($\mu$g N m$^{-3}$) | Canopy compensation point |

to the value of $\beta$ and it is able to represent the main temporal development of ammonia emission even with 0 buffering capacity.

On the other hand, we found that incorporating a simple estimation of $CO_2$ emission allows the model to reproduce the measured soil pH values more accurately than neglecting $CO_2$ emissions. Future work should therefore consider how $CO_2$ fluxes could be incorporated more systematically into the GAG model.

The model turned out to be sensitive to the value of soil water content at field capacity ($\theta_{fc}$) and at permanent wilting point ($\theta_{pwp}$). Thus, at regional scale application, where mostly recommended values of these parameters are available, this error has to be considered when interpreting the model results.

Our results support the vital role of temperature in $NH_3$ exchange, showing a high correlation with the temperature parameters as well as strong sensitivity to them. Nevertheless, the GAG model provides only a modest overall temperature dependence in total $NH_3$ emission compared to what was reported in the literature earlier. A possible explanation for this is that, according to our results, the sensitivity to temperature is higher close to urine application than in the later stages and may depend also on interactions with other nitrogen cycling processes.

In addition, we found that wind speed and relative humidity are also significant influencing factors. In the case of RH we observed a dual effect through its effect on the modelled soil evaporation and the modelled deposition to leaf surfaces, with the latter being the dominant term for the present simulations.

In contrast to the $NH_3$ volatilization models published earlier for urea affected soils (Sherlock and Goh, 1985; Rachhpal and Nye, 1986), our model, incorporating a canopy compensation point model, accounts for the effect of the meteorological parameters on net canopy exchange of $NH_3$. Compared with the model constructed by Laubach et al. (2012), GAG is capable of simulating the influence of vegetation on $NH_3$ exchange. In addition, our model also simulates soil pH, the TAN and the water content of the soil, allowing it to predict net $NH_3$ emission, instead of operating only in "inverse" mode, calculating soil parameters based on flux measurements.

Rachhpal and Nye (1986) suggested a solution for dynamic modelling of soil pH with a set of continuity equations. However, in their approach the dissociation coefficients, as well as the urea hydrolysis rate, were independent of temperature. Even though the GAG model accounts for the same chemical reactions, it incorporates a different mathematical description and accounts for the missing temperature dependencies.

Dynamic simulation of soil pH is novel among the $NH_3$ exchange models on the ecosystem scale. In the PaSim ecosystem model (Riedo et al., 2002) pH is treated as a constant, and the same is true for the VOLT'AIR model (Géner-

mont and Cellier, 1997) developed for simulating $NH_3$ emission related to fertilizer and manure application. Furthermore, the framework of GAG is simpler and requires less input data than the VOLT'AIR model. Therefore, for grazing situations, it is much easier to adapt GAG on both field and regional scale.

As our final goal is to apply the model to regional scale, simplicity was a key aspect of the model development, avoiding extra steps of model simplification in the later stages of our project. Therefore, the model operates with a single layer approach in the soil. Although this is a simpler approach compared to some of the above-mentioned models (Rachhpal and Nye, 1986; Génermont and Cellier, 1997; Riedo et al., 2002), the model code is easily amendable, which enables us to add new modules to GAG in the future.

Since all the input parameters can be obtained for larger scales, considering the possible errors, GAG is concluded to be suitable for larger-scale application, such as in regional atmospheric and ecosystem models. In addition, as it is dynamically driven by weather parameters, it can serve as a base for further studies of climate dependency of ammonia emission from grazed fields on both plot and regional scale.

## 8   Conclusions

We report the description of a process-based, weather-driven ammonia exchange model for a urine patch that is capable of simulating the TAN and the water content of the soil under a urine patch and also soil pH.

The model tests suggest that ammonia volatilization from a urine patch can be affected by the possible restart of urea hydrolysis after a rain event as well as $CO_2$ emission from the soil.

The vital role of temperature in $NH_3$ exchange is supported by our model results; however, the GAG model provides only a modest overall temperature dependence in total $NH_3$ emission compared with the literature. This, according to our findings, can be explained by the higher sensitivity to temperature close to urine application than in the later stages and may depend on interactions with other nitrogen cycling processes. In addition, we found that wind speed and relative humidity are also significant influencing factors. These relationships need to be further tested in relation to field measurements.

For simplicity, to allow subsequent regional upscaling, the model operates with a single soil layer approach, neglecting water movement and solution mixing in the soil. Although this is a limitation of the current model version, the model code is easily amendable, which facilitates to add new modules to GAG in the future.

Considering that all the input parameters can be obtained for larger scales, GAG is potentially suitable for field and regional scale application, serving as a tool for further investi-

gation of the effects of climate change on ammonia emissions and deposition.

## The Supplement related to this article is available online at doi:10.5194/bg-13-1837-2016-supplement.

## References

Allen, R. G., Pereira, L. S., Raes, D., and Smith, M.: Crop evapotranspiration-Guidelines for computing crop water requirements, FAO Irrigation and drainage paper 56, FAO, Rome, Italy, 1998.

Bates, R. G. and Pinching, G. D.: Acidic dissociation constant of ammonium ion at $0\,°C$ to $50\,°C$, and the base strength of ammonia, J. Res. Nat. Bur. Stand., 42, 419–430, doi:10.6028/jres.042.037, 1949.

Betteridge, K., Andrewes, W. G. K., and Sedcole, J. R.: Intake and excretion of nitrogen, potassium and phosporus by grazing steers, J. Agr. Sci., 106, 393–404, 1986.

Burkhardt, J., Kaiser, H., Goldbach, H., and Kappen, L.: Measurements of electrical leaf surface conductance reveal re-condensation of transpired water vapour on leaf surfaces, Plant Cell Environ., 22, 189–196, doi:10.1046/j.1365-3040.1999.00387.x, 1999.

Burkhardt, J., Flechard, C. R., Gresens, F., Mattsson, M., Jongejan, P. A. C., Erisman, J. W., Weidinger, T., Meszaros, R., Nemitz, E., and Sutton, M. A.: Modelling the dynamic chemical interactions of atmospheric ammonia with leaf surface wetness in a managed grassland canopy, Biogeosciences, 6, 67–84, doi:10.5194/bg-6-67-2009, 2009.

Cooter, E. J., Bash, J. O., Walker, J. T., Jones, M. R., and Robarge, W.: Estimation of $NH_3$ bi-directional flux from managed agricultural soils, Atmos. Environ., 44, 2107–2115, doi:10.1016/j.atmosenv.2010.02.044, 2010.

Dasgupta, P. K. and Dong, S.: Solubility of ammonia in liquid water and generation of trace levels of standard gaseous ammonia, Atmos. Environ., 20, 565–570, doi:10.1016/0004-6981(86)90099-5, 1986.

Dijkstra, J., Oenema, O., van Groenigen, J. W., Spek, J. W., van Vuuren, A. M., and Bannink, A.: Diet effects on urine composition of cattle and $N_2O$ emissions, Animal, 7, 292–302, doi:10.1017/S1751731113000578, 2013.

Doak, B. W.: Some chemical changes in the nitrogenous constituents of urine when voided on pasture, J. Agr. Sci., 42, 162–171, 1952.

EDGAR: Emissions Database for Global Atmospheric Research v4.2, available at: http://edgar.jrc.ec.europa.eu/ (last access: 20 May 2014), 2011.

Emberson, L., Simpson, D., Tuovinen, J.-P., Ashmore, M., and Cambridge, H.: Towards a model of ozone deposition and stomatal uptake over Europe, EMEP MSC-W Note 6/2000, The Norwegian Meteorological Institute, Oslo, Norway, 2000.

Farquhar, G. D., Firth, P. M., Wetselaar, R., and Weir, B.: On the Gaseous Exchange of Ammonia between Leaves and the Environment: Determination of the Ammonia Compensation Point, Plant. Physiol., 66, 710–714, doi:10.1104/pp.66.4.710, 1980.

Flechard, C. R., Fowler, D., Sutton, M. A., and Cape, J. N.: A dynamic chemical model of bi-directional ammonia exchange between semi-natural vegetation and the atmosphere, Q. J. Roy. Meteor. Soc., 125, 2611–2641, doi:10.1002/qj.49712555914, 1999.

Flechard, C. R., Massad, R.-S., Loubet, B., Personne, E., Simpson, D., Bash, J. O., Cooter, E. J., Nemitz, E., and Sutton, M. A.: Advances in understanding, models and parameterizations of biosphere-atmosphere ammonia exchange, Biogeosciences, 10, 5183–5225, doi:10.5194/bg-10-5183-2013, 2013.

Fowler, D., Coyle, M., Skiba, U., Sutton, M. A., Cape, J. N., Reis, S., Sheppard, L. J., Jenkins, A., Grizzetti, B., Galloway, J. N., Vitousek, P., Leach, A., Bouwman, A. F., Butterbach-Bahl, K., Dentener, F., Stevenson, D., Amann, M., and Voss, M.: The global nitrogen cycle in the twenty-first century, Philos. T. R. Soc. B, 368, 20130164, doi:10.1098/rstb.2013.0164, 2013.

Galloway, J. N., Townsend, A. R., Erisman, J. W., Bekunda, M., Cai, Z., Freney, J. R., Martinelli, L. A., Seitzinger, S. P., and Sutton, M. A.: Transformation of the Nitrogen Cycle: Recent Trends, Questions, and Potential Solutions, Science, 320, 889–892, doi:10.1126/science.1136674, 2008.

Génermont, S. and Cellier, P.: A mechanistic model for estimating ammonia volatilization from slurry applied to bare soil, Agr. Forest Meteorol., 88, 145–167, doi:10.1016/S0168-1923(97)00044-0, 1997.

Harned, H. S. and Davis, R.: The Ionization Constant of Carbonic Acid in Water and the Solubility of Carbon Dioxide in Water and Aqueous Salt Solutions from 0 to 50°, J. Am. Chem. Soc., 65, 2030–2037, doi:10.1021/ja01250a059, 1943.

Harned, H. S. and Scholes, S. R.: The Ionization Constant of $HCO_3^-$ from 0 to 50°, J. Am. Chem. Soc., 63, 1706–1709, doi:10.1021/ja01851a058, 1941.

Hellsten, S., Dragosits, U., Place, C. J., Vieno, M., Dore, A. J., Misselbrook, T. H., Tang, Y. S., and Sutton, M. A.: Modelling the spatial distribution of ammonia emissions in the UK, Environ. Pollut., 154, 370–379, doi:10.1016/j.envpol.2008.02.017, 2008.

Hicks, B. B., Baldocchi, D. D., Meyers, T. P., Hosker Jr., R. P., and Matt, D. R.: A preliminary multiple resistance routine for deriving dry deposition velocities from measured quantities, Water Air Soil Pollut., 36, 311–330, doi:10.1007/BF00229675, 1987.

Hoogendoorn, C. J., Betteridge, K., Costall, D. A., and Ledgard, S. F.: Nitrogen concentration in the urine of cattle, sheep and deer grazing a common ryegrass/cocksfoot/white clover pasture, New Zealand, J. Agr. Res., 53, 235–243, doi:10.1080/00288233.2010.499899, 2010.

Horváth, L., Asztalos, M., Führer, E., Mészáros, R., and Weidinger, T.: Measurement of ammonia exchange over grassland in the

Hungarian Great Plain, Agr. Forest Meteorol., 130, 282–298, doi:10.1016/j.agrformet.2005.04.005, 2005.

Kielland, J.: Individual Activity Coefficients of Ions in Aqueous Solutions, J. Am. Chem. Soc., 59, 1675–1678, doi:10.1021/ja01288a032, 1937.

Laubach, J., Taghizadeh-Toosi, A., Sherlock, R. R., and Kelliher, F. M.: Measuring and modelling ammonia emissions from a regular pattern of cattle urine patches, Agr. Forest Meteorol., 156, 1–17, doi:10.1016/j.agrformet.2011.12.007, 2012.

Laubach, J., Taghizadeh-Toosi, A., Gibbs, S. J., Sherlock, R. R., Kelliher, F. M., and Grover, S. P. P.: Ammonia emissions from cattle urine and dung excreted on pasture, Biogeosciences, 10, 327–338, doi:10.5194/bg-10-327-2013, 2013.

Leuning, R., Freney, J. R., Denmead, O. T., and Simpson, J. R.: A sampler for measuring atmospheric ammonia flux, Atmos. Environ., 19, 1117–1124, doi:10.1016/0004-6981(85)90196-9, 1985.

Lin, X., Wang, S., Ma, X., Xu, G., Luo, C., Li, Y., Jiang, G., and Xie, Z.: Fluxes of $CO_2$, $CH_4$, and $N_2O$ in an alpine meadow affected by yak excreta on the Qinghai-Tibetan plateau during summer grazing periods, Soil Biol. Biochem., 41, 718–725, doi:10.1016/j.soilbio.2009.01.007, 2009.

Ma, X., Wang, S., Wang, Y., Jiang, G., and Nyren, P.: Short-term effects of sheep excrement on carbon dioxide, nitrous oxide and methane fluxes in typical grassland of Inner Mongolia, New Zealand, J. Agr. Res., 49, 285–297, 2006.

Massad, R.-S., Tuzet, A., Loubet, B., Perrier, A., and Cellier, P.: Model of stomatal ammonia compensation point (STAMP) in relation to the plant nitrogen and carbon metabolisms and environmental conditions, Ecol. Model., 221, 479–494, doi:10.1016/j.ecolmodel.2009.10.029, 2010a.

Massad, R.-S., Nemitz, E., and Sutton, M. A.: Review and parameterisation of bi-directional ammonia exchange between vegetation and the atmosphere, Atmos. Chem. Phys., 10, 10359–10386, doi:10.5194/acp-10-10359-2010, 2010b.

Millington, R. J. and Quirk, J. P.: Permeability of porous solids, T. Faraday Soc., 57, 1200–1207, doi:10.1039/tf9615701200, 1961.

Misselbrook, T. H., Gilhespy, S. L., Cardenas, L. M., Chambers, B. J., Smith, K. A., Williams, J., and Dragosits, U.: Inventory of Ammonia Emissions from UK Agriculture, Inventory Submission Report, DEFRA, London, UK, 2012.

Nemitz, E., Sutton, M. A., Schjoerring, J. K., Husted, S., and Paul Wyers, G.: Resistance modelling of ammonia exchange over oilseed rape, Agr. Forest Meteorol., 105, 405–425, doi:10.1016/S0168-1923(00)00206-9, 2000.

Nemitz, E., Milford, C., and Sutton, M. A.: A two-layer canopy compensation point model for describing bi-directional biosphere-atmosphere exchange of ammonia, Q. J. Roy. Meteor. Soc., 127, 815–833, doi:10.1256/smsqj.57305, 2001.

NIWA: The National Climate Database, available at: http://cliflo.niwa.co.nz/ (last access: 2 December 2013), 2015.

Petersen, S. O., Sommer, S. G., Aaes, O., and Søegaard, K.: Ammonia losses from urine and dung of grazing cattle: effect of N intake, Atmos. Environ., 32, 295–300, doi:10.1016/S1352-2310(97)00043-5, 1998.

R Core Team: R: A language and environment for statistical computing. R Foundation for Statistical Computing, Vienna, Austria, 2012.

Rachhpal, S. and Nye, P. H.: A model of ammonia volatilization from applied urea. I. Development of the model, J. Soil Sci., 37, 9–20, doi:10.1111/j.1365-2389.1986.tb00002.x, 1986.

Riddick, S. N.: Global ammonia emissions from seabird colonies, Ph.D. thesis, Kings College, London, UK, 2012.

Riedo, M., Milford, C., Schmid, M., and Sutton, M. A.: Coupling soil–plant–atmosphere exchange of ammonia with ecosystem functioning in grasslands, Ecol. Model., 158, 83–110, doi:10.1016/S0304-3800(02)00169-2, 2002.

Sherlock, R. R. and Goh, K. M.: Dynamics of ammonia volatilization from simulated urine patches and aqueous urea applied to pasture I. Field experiments, Fert. Res., 5, 181–195, doi:10.1007/BF01052715, 1984.

Sherlock, R. R. and Goh, K. M.: Dynamics of ammonia volatilization from simulated urine patches and aqueous urea applied to pasture, II. Theoretical derivation of a simplified model, Fert. Res., 6, 3–22, doi:10.1007/BF01058161, 1985.

Shorten, P. R. and Pleasants, A. B.: A stochastic model of urinary nitrogen and water flow in grassland soil in New Zealand, Agric. Ecosyst. Environ., 120, 145–152, doi:10.1016/j.agee.2006.08.017, 2007.

Simpson, D., Benedictow, A., Berge, H., Bergström, R., Emberson, L. D., Fagerli, H., Flechard, C. R., Hayman, G. D., Gauss, M., Jonson, J. E., Jenkin, M. E., Nyíri, A., Richter, C., Semeena, V. S., Tsyro, S., Tuovinen, J.-P., Valdebenito, Á., and Wind, P.: The EMEP MSC-W chemical transport model – technical description, Atmos. Chem. Phys., 12, 7825–7865, doi:10.5194/acp-12-7825-2012, 2012.

Sutton, M. A. and Fowler, D.: A model for inferring bi-directional fluxes of ammonia over plant canopies, in: WMO Conference on the Measurement and Modeling of Atmospheric Composition Changes including Pollution Transport, WMO/GAW-91, Sofia, Bulgaria, 4–8 October 1993, WMO, Geneva, 179–182, 1993.

Sutton, M. A., Schjorring, J. K., and Wyers, G. P.: Plant-Atmosphere Exchange of Ammonia, Philos. T. R. Soc. A, 351, 261–276, doi:10.1098/rsta.1995.0033, 1995.

Sutton, M. A., Howard, C. M., Erisman, J. W., Bealey, W. J., Billen, G., Bleeker, A., Bouwman, A. F., Grennfelt, P., van Grinsven, H., and Grizzetti, B.: The challenge to integrate nitrogen science and policies: the European Nitrogen Assessment approach, in: The European Nitrogen Assessment: Sources, Effects and Policy Perspectives, edited by: Sutton, M. A., Howard, C. M., Erisman, J. W., Billen, G., Bleeker, A., Grennfelt, P., Van Grinsven, H., and Grizzetti, B., Cambridge University Press, Cambridge, UK, 82–96, 2011.

Sutton, M. A., Reis, S., Riddick, S. N., Dragosits, U., Nemitz, E., Theobald, M. R., Tang, Y. S., Braban, C. F., Vieno, M., Dore, A. J., Mitchell, R. F., Wanless, S., Daunt, F., Fowler, D., Blackall, T. D., Milford, C., Flechard, C. R., Loubet, B., Massad, R., Cellier, P., Personne, E., Coheur, P. F., Clarisse, L., Van Damme, M., Ngadi, Y., Clerbaux, C., Skjøth, C. A., Geels, C., Hertel, O., Wichink Kruit, R. J., Pinder, R. W., Bash, J. O., Walker, J. T., Simpson, D., Horváth, L., Misselbrook, T. H., Bleeker, A., Dentener, F., and de Vries, W.: Towards a climate-dependent paradigm of ammonia emission and deposition, Philos. T. R. Soc. B, 368, 20130166, doi:10.1098/rstb.2013.0166, 2013.

Vieno, M., Dore, A. J., Stevenson, D. S., Doherty, R., Heal, M. R., Reis, S., Hallsworth, S., Tarrason, L., Wind, P., Fowler, D., Simpson, D., and Sutton, M. A.: Modelling surface ozone during the

2003 heat-wave in the UK, Atmos. Chem. Phys., 10, 7963–7978, doi:10.5194/acp-10-7963-2010, 2010.

Vieno, M., Heal, M. R., Hallsworth, S., Famulari, D., Doherty, R. M., Dore, A. J., Tang, Y. S., Braban, C. F., Leaver, D., Sutton, M. A., and Reis, S.: The role of long-range transport and domestic emissions in determining atmospheric secondary inorganic particle concentrations across the UK, Atmos. Chem. Phys., 14, 8435–8447, doi:10.5194/acp-14-8435-2014, 2014.

Walter, I., Allen, R., Elliott, R., Jensen, M., Itenfisu, D., Mecham, B., Howell, T., Snyder, R., Brown, P., Echings, S., Spofford, T., Hattendorf, M., Cuenca, R., Wright, J., and Martin, D.: ASCE's Standardized Reference Evapotranspiration Equation, in: Watershed Management and Operations Management 2000, American Society of Civil Engineers, Fort Collins, Colorado, US, 20–24 June 2000, 1–11, 2001.

Wang, X., Huang, D., Zhang, Y., Chen, W., Wang, C., Yang, X., and Luo, W.: Dynamic changes of $CH_4$ and $CO_2$ emission from grazing sheep urine and dung patches in typical steppe, Atmos. Environ., 79, 576–581, doi:10.1016/j.atmosenv.2013.07.003, 2013.

Whitehead, D. C. and Raistrick, N.: The volatilization of ammonia from cattle urine applied to soils as influenced by soil properties, Plant Soil, 148, 43–51, doi:10.1007/BF02185383, 1993.

Whitehead, D. C., Lockyer, D. R., and Raistrick, N.: Volatilization of ammonia from urea applied to soil: Influence of hippuric acid and other constituents of livestock urine, Soil Biol. Biochem., 21, 803–808, doi:10.1016/0038-0717(89)90174-0, 1989.

Wilhelm, E., Battino, R., and Wilcock, R. J.: Low-pressure solubility of gases in liquid water, Chem. Rev., 77, 219–262, doi:10.1021/cr60306a003, 1977.

Wu, Y., Walker, J., Schwede, D., Peterslidard, C., Dennis, R., and Robarge, W.: A new model of bi-directional ammonia exchange between the atmosphere and biosphere: Ammonia stomatal compensation point, Agr. Forest Meteorol., 149, 263–280, doi:10.1016/j.agrformet.2008.08.012, 2009.